AFRL-RX-TY-TR-2010-0095

PRECAST CONCRETE PANELS FOR CONTINGENCY RIGID AIRFIELD PAVEMENT DAMAGE REPAIRS

Reza S. Ashtiani, Christopher J. Jackson and Athar Saeed
Applied Research Associates, Inc.
421 Oak Avenue
Panama City, FL 32401

Michael I. Hammons
Airbase Technologies Division
Air Force Research Laboratory
139 Barnes Drive, Suite 2
Tyndall Air Force Base, FL 32403-5323

Contract No. FA4819-09-C-0028

June 2010

AIR FORCE RESEARCH LABORATORY
MATERIALS AND MANUFACTURING DIRECTORATE

■ **Air Force Materiel Command** ■ **United States Air Force** ■ **Tyndall Air Force Base, FL 32403-5323**

NOTICE AND SIGNATURE PAGE

Using Government drawings, specifications, or other data included in this document for any purpose other than Government procurement does not in any way obligate the U.S. Government. The fact that the Government formulated or supplied the drawings, specifications, or other data does not license the holder or any other person or corporation; or convey any rights or permission to manufacture, use, or sell any patented invention that may relate to them.

This report was cleared for public release by the 88th Air Base Wing Public Affairs Office at Wright Patterson Air Force Base, Ohio and is available to the general public, including foreign nationals. Copies may be obtained from the Defense Technical Information Center (DTIC) (http://www.dtic.mil).

AFRL-RX-TY-TR-2010-0095 HAS BEEN REVIEWED AND IS APPROVED FOR PUBLICATION IN ACCORDANCE WITH ASSIGNED DISTRIBUTION STATEMENT.

CUBILLOS FONSECA.ANGELICA.NMN .1258842541
Digitally signed by CUBILLOS FONSECA.ANGELICA.NMN.1258842541
DN: c=US, o=U.S. Government, ou=DoD, ou=PKI, ou=USAF, cn=CUBILLOS FONSECA.ANGELICA.NMN.1258842541
Date: 2011.05.31 09:48:17 -05'00'

ANGELICA CUBILLOS, 2d Lt, USAF
Work Unit Manager

RICHLIN.DEBRA.L .1034494149
Digitally signed by RICHLIN.DEBRA.L.1034494149
DN: c=US, o=U.S. Government, ou=DoD, ou=PKI, ou=USAF, cn=RICHLIN.DEBRA.L.1034494149
Date: 2011.05.30 03:12:23 -05'00'

DEBRA L. RICHLIN, DR-III
Acting Chief, Airbase Engineering Development Branch

PILSON.DONNA.L .1186939324
Digitally signed by PILSON.DONNA.L.1186939324
DN: c=US, o=U.S. Government, ou=DoD, ou=PKI, ou=USAF, cn=PILSON.DONNA.L.1186939324
Date: 2012.04.03 11:17:51 -05'00'

DONNA L. PILSON, LtCol, USAF
Deputy Chief, Airbase Technologies Division

This report is published in the interest of scientific and technical information exchange, and its publication does not constitute the Government's approval or disapproval of its ideas or findings.

REPORT DOCUMENTATION PAGE

Form Approved
OMB No. 0704-0188

PLEASE DO NOT RETURN YOUR FORM TO THE ABOVE ADDRESS.

1. REPORT DATE *(DD-MM-YYYY)*	2. REPORT TYPE	3. DATES COVERED *(From - To)*
30-JUN-2010	Final Technical Report	01-JAN-2008 -- 30-APR-2010

4. TITLE AND SUBTITLE

Pre-Cast Concrete Panels for Rapid Repair of Airfield Rigid Pavements

5a. CONTRACT NUMBER

FA4819-09-C-0028

5b. GRANT NUMBER

5c. PROGRAM ELEMENT NUMBER

62102F

6. AUTHOR(S)

*Ashtiani, Reza S.; *Jackson, Christopher J.; *Saeed, Athar; **Hammons, Michael I.

5d. PROJECT NUMBER

4915

5e. TASK NUMBER

D1

5f. WORK UNIT NUMBER

4915D14E

7. PERFORMING ORGANIZATION NAME(S) AND ADDRESS(ES)

* Applied Research Associates
421 Oak Avenue
Panama City, FL 32401

8. PERFORMING ORGANIZATION REPORT NUMBER

9. SPONSORING/MONITORING AGENCY NAME(S) AND ADDRESS(ES)

** Air Force Research Laboratory
Materials and Manufacturing Directorate
Airbase Technologies Division
139 Barnes Drive, Suite 2
Tyndall Air Force Base, FL 32403-5323

10. SPONSOR/MONITOR'S ACRONYM(S)

AFRL/RXQEM

11. SPONSOR/MONITOR'S REPORT NUMBER(S)

AFRL-RX-TY-TR-2010-0095

12. DISTRIBUTION/AVAILABILITY STATEMENT

Distribution Statement A: Approved for public release; distribution unlimited.

13. SUPPLEMENTARY NOTES

Ref Public Affairs Case # 88ABW-2012-2057, 6 April 2012. Document contains color images.

14. ABSTRACT

Significant number of airfield pavements are constructed with Portland Cement Concrete (PCC). Effectively restoring damaged PCC sections in military airfields requires a well-formulated repair plan. This study investigates the feasibility and efficiency of using different precast concrete panel installation techniques for contingency repair of damaged airfield pavements. High-density polyurethane (HDP) foam and flowable fill were selected as bedding and leveling materials after literature review. Deep injection using HDP foam as well as conventional leveling using cement mortar were investigated to determine the impact of leveling techniques on repair performance. Performance of the repaired sections was characterized by load transfer efficiency, joint stiffness and deformation energy dissipated through the pavement foundation. A heavy weight deflectometer (HWD) along with an F-15 gear simulator was used to determine the stiffness properties and accumulation of plastic deformations after each load interval during performance testing. Decay of joint stiffness and load transfer efficiency, as well as increase in deformation energy, were calculated as a function of number of load applications. The results indicate a significant increase in the deformation energy and considerable loss of joint stiffness with number of load applications when flowable fill was used as leveling material. This study reveals that precast panels installed with HDP foam performed superior compared to precast panels installed with flowable fill. Additionally, precast panels installed using deep injection method performed better in terms of higher load transfer efficiency, higher joint stiffness and lower dissipated deformation energy. This study suggests that precast concrete panels leveled using HDP foam deep injection method outperformed other investigated permutations.

15. SUBJECT TERMS

pre-cast, pre-cast concrete, concrete panels, rapid concrete repair, airfield repair, airfield rigid pavements

16. SECURITY CLASSIFICATION OF:			17. LIMITATION OF ABSTRACT	18. NUMBER OF PAGES	19a. NAME OF RESPONSIBLE PERSON
a. REPORT	b. ABSTRACT	c. THIS PAGE			Angelica Cubillos
U	U	U	UU	85	19b. TELEPHONE NUMBER *(Include area code)*

Reset

Standard Form 298 (Rev. 8/98)
Prescribed by ANSI Std. Z39.18

TABLE OF CONTENTS

LIST OF FIGURES

LIST OF TABLES

Page

1. EXECUTIVE SUMMARY

Significant numbers of airfield pavements are constructed with Portland cement concrete (PCC). Effectively restoring damaged PCC sections in military airfields requires a well-formulated repair plan. This study investigates the feasibility and efficiency of using different precast concrete panel installation techniques for contingency repair of damaged airfield pavements. High-density polyurethane (HDP) foam and flowable fill were selected as bedding and leveling materials after the literature review. Deep injection using HDP foam as well as conventional leveling using cement mortar were investigated to determine the impact of leveling techniques on repair performance.

Performance of the repaired sections was characterized by load transfer efficiency (LTE), joint stiffness and deformation energy dissipated through the pavement foundation. A heavy-weight deflectometer (HWD) along with an F-15 gear simulator were used to determine the stiffness properties and accumulation of plastic deformations after each load interval during performance testing. Decay of joint stiffness and LTE, as well as increase in deformation energy, were calculated as a function of number of load applications. The results indicated a significant increase in the deformation energy and considerable loss of joint stiffness with increasing numbers of load applications when flowable fill was used as leveling material. This study reveals that precast panels installed with HDP foam performed superior compared to precast panels installed with flowable fill. Additionally, precast panels installed using deep injection method performed better in terms of higher LTE, higher joint stiffness and lower dissipated deformation energy. This study suggests that precast concrete panels leveled using HDP foam deep injection method outperformed other investigated permutations.

2. INTRODUCTION

The ability to rapidly repair damaged airfield sections is of paramount importance. It is imperative to restore flight operations in the shortest possible time. Currently, there are several methods for expedient repairs of damaged PCC airfield sections. One method uses cast-in-place, high-early-strength concrete. The cast-in-place procedure entails completely removing the damaged portion of PCC airfield pavement and subsequently placing fresh concrete into the resulting void. The cast-in-place method is labor intensive and requires skilled personnel. A second method involves the use of precast concrete panels. The precast concrete panel procedure requires removing a damaged section of runway and replacing the damaged section with one or more precast panels. Obviously, the designated repair area from the removed damaged section and the precast section must be congruent.

2.1. Background

A significant number of military airfields are constructed with PCC. PCC runways, aprons, and taxiways have a finite service life that depends on several factors. These factors include aircraft landing type and frequency, condition of base-course and subgrade, and environmental and temperature conditions.

PCC degradation progresses with accumulation of traffic (load) and weather stresses. Minor repairs can be accomplished with limited or no traffic interruption. However, repairing pavement areas encompassing single or multiple slabs requires planning and special techniques to minimize the impact to aircraft operations.

Rapid repair techniques for rigid pavements are methodologies intended to reduce airfield operational delays. These techniques, also known as fast-track construction, have become a prevalent component of pavement engineering. Fast-track repairs are best described as a comprehensive effort to expedite the logistical and physical aspects of the construction schedule.

2.2. Fast Track Rigid Pavement Repair

Severely damaged rigid pavements are often rehabilitated using full-depth repair techniques. These techniques involve removing the entire thickness of the damaged PCC slab and replacing it with a new slab. The traditional, cast-in-place method, utilizes high-early-strength rapid-setting concrete. The cast-in-place procedure entails completely removing the damaged portion of airfield pavement and subsequently placing fresh concrete into the resulting void. These slabs can support traffic loading in as little as 2 to 4 hours [1]. However, high-early-strength rapid-setting concrete may not be as durable as traditional concrete and its placement requires favorable weather conditions.

Fast-track repair methods, utilizing precast concrete panels, provide a viable alternative to the cast-in-place method. The precast repair method involves removing the damaged section of the PCC pavement and replacing it with a precast congruent concrete panel. This is typically accomplished by saw-cutting a portion of the existing slab containing the damaged section, and placing the precast concrete panel into the removed area. It is essential to tie the precast panel to the existing concrete pavement to facilitate load transfer across the joint, which is generally

accomplished by connecting reinforcement dowel rods from the precast concrete panel to the existing slabs.

2.3. Advantages and Disadvantages of Precast Concrete Panel Repair

Precast concrete panels allow for expedited PCC pavement repairs. In optimal conditions, it is possible to complete a single panel repair and subject the repaired section to traffic in less than 6 hours [2]. Conversely, traditional cast-in-place repairs using conventional PCC may require several weeks of closure due to the time required for the PCC to achieve adequate strength. Similarly, high-early-strength rapid-setting cast-in-place PCC repair requires several hours of closure due to the time required to achieve adequate strength. The window of permissible weather for the installation of precast panels is perhaps wider than that for fast-track repairs using cast-in-place high-early-strength concrete [2]. When an expedited installation is required, the traditional cast-in-place method does not provide an acceptable alternative and the weather window essential for fast-track cast-in-place repairs may not be available, then precast concrete panels are recommended.

Advantages of utilizing precast concrete panels, as opposed to high-early-strength rapid-setting concrete, include the following:

a) **Improved Quality Control:**
   Precast concrete panels can be manufactured in a controlled environment. This allows for a suite of concrete mechanical properties analysis before installation. Additionally, pre-manufacturing the replacement sections affords the opportunity to texture the exposed surface in a clinical environment.
b) **Precast Panels Can Be Stored on Site Until Needed:**
   Precast concrete panels can be pre-manufactured and stored on site, eliminating the need to transfer panels from a remote location. Stored panels can be utilized for emergency repair. This advantage is most apparent when the possible repair dimensions are predictable.
c) **Wide Weather Window:**
   The weather window required for installation of precast panels may be significantly larger than the window necessary for fast-track cast-in-place repairs. Temperature concerns are mitigated with precast panel repair because the concrete has previously cured in a controlled environment. Precipitations issues are also mitigated due to the fact that the cured concrete panels are not water sensitive. Grouting materials used to tie the panels to the existing slab and level the precast panel are typically water-sensitive, but in many situations the repaired area can be trafficked on a temporary basis before grout placement.

There are disadvantages associated with precast panel repair. The most obvious is cost, though economies of scale should help minimize expenses. Transportation agencies have estimated that the cost of precast concrete panel repair can be 1.6 to 4 times more than cast-in-place repair options [2]. Additionally, the precast repair method is a relatively recent technology. There is limited performance data available and load transfer and longevity concerns exist.

2.4. Types of Repairs

Full-depth precast concrete panel repair is separated into two distinct repair types: single panel repair and connected panel repair.

2.4.1. Single Panel Repair

Single panel repair is characterized by the replacement of a single panel. Dowel rods are utilized to integrate the panel into the surrounding concrete matrix; however, care should be exercised to ensure that slab movement (expansion/contraction) is not restricted. Single panel repair is practical when the entire damaged area of the existing slab is smaller than individual precast concrete panels. In some situations, several single repair panels may be interspersed on the existing concrete slab. Figure 1 illustrates a possible single panel repair scenario.

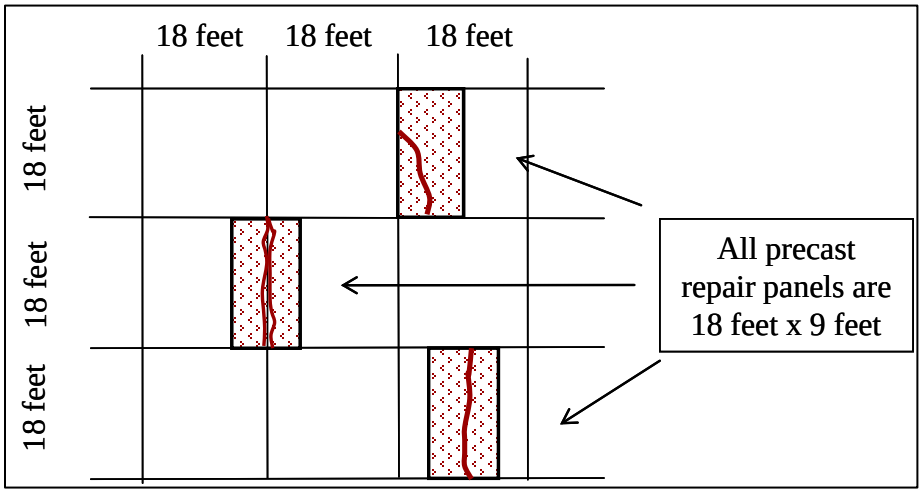

Figure 1. Single Precast Panel Repair Scenario [2]

2.4.2. Connected Panel Repair

Connected panel repair is characterized by the replacement of multiple, connected panels. Dowel rods are used as load transfer mechanisms. The dowel rods tie the precast panels to each other and the existing slab. Connected panel repair is practical when the extent of the damaged area exceeds the size of a single panel. Figure 2 illustrates a possible connected panel repair scenario.

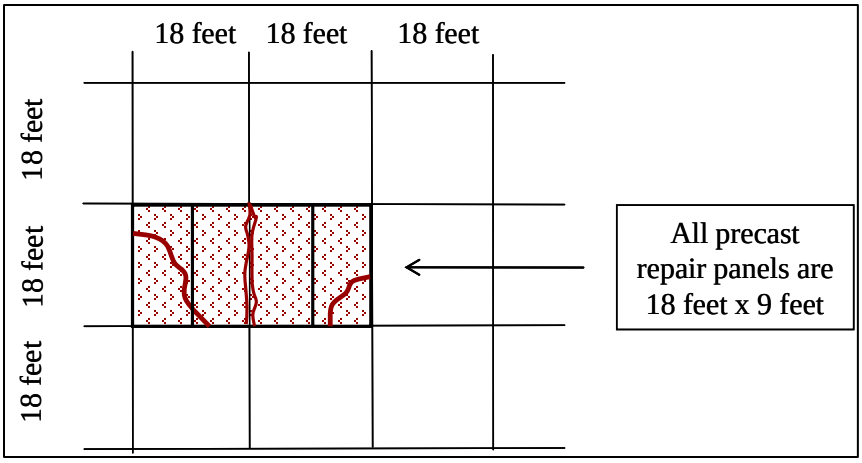

Figure 2. Connected Precast Panel Repair Scenario [2]

2.5. Precast Panel Repair Methodologies

There are several precast concrete panel repair methodologies. The most common include the Fort Miller Super-Slab® Method, the Michigan Method and the URETEK Method. Alternative methods incorporate elements from each of these three methods [2]. The delineations between the aforementioned methods are exhibited in the approach to load transfer and base support.

2.5.1. Fort Miller Super-Slab® Method

Fort Miller Super-Slab® Method is a patented method. Usually, local contractors work in conjunction with a Fort Miller representative to complete these repairs. Fort Miller repairs include both single panel and connected panel replacement (Figure 3).

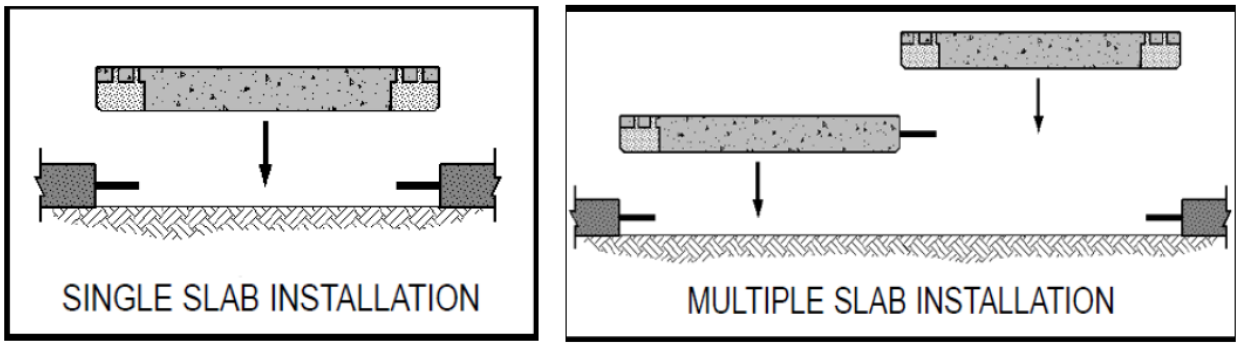

Figure 3. Fort Miller Precast Concrete Panel Repairs [3]

2.5.1.1. Load Transfer

The Fort Miller method's approach to load transfer is to manufacture precast concrete panels with dowel slots on the bottom of the panel [3]. Load transfer dowel rods are pre-installed in the existing pavement (Figure 4). The configuration of the pre-installed dowel rods allows for the dowel slots to fit over them. Grout ports provide an opportunity to grout the dowel rods after placement of the precast concrete panel (Figure 5).

Figure 4. Installation of Load Transfer Dowel Rods into the Existing Rigid Pavement [3]

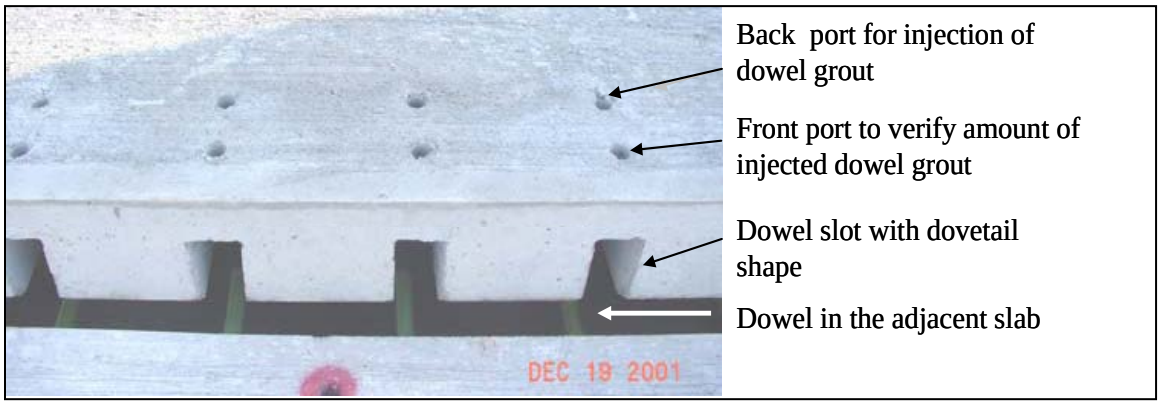

Figure 5. Grout Installation Ports [3]

2.5.1.2. Base Preparation

After compaction of the base course material, a ¾-inch thick layer of fine mineral aggregate is spread over the base. The layer is then compacted and precision leveled with a mechanical screeding device (Figure 6). After screeding the base and grouting the load transfer dowel rods into place, bedding grout is injected under the panel. The distribution of the bedding grout is facilitated by bedding grout distribution channels on the underside of the panel (Figure 7).

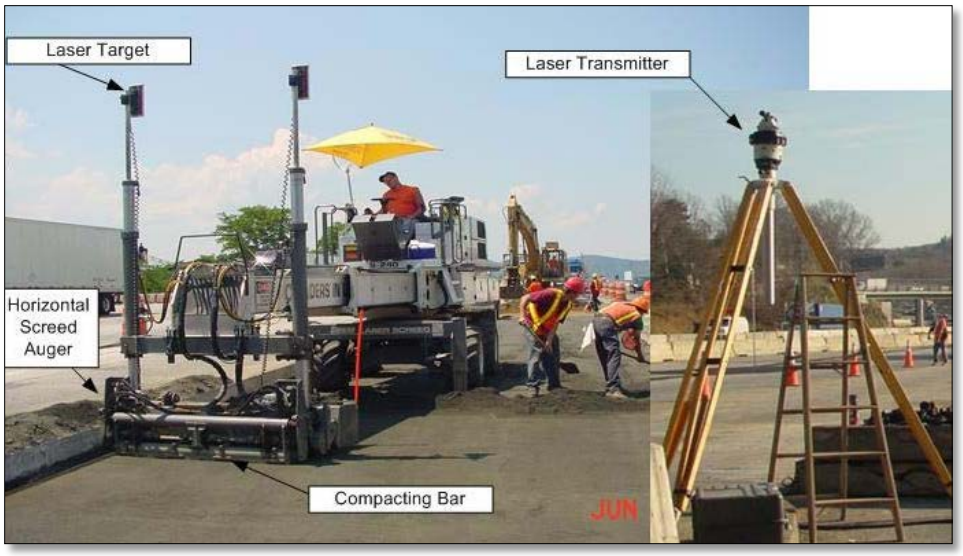

Figure 6. Fort Miller Super-Slab® Method Base Preparation [3]

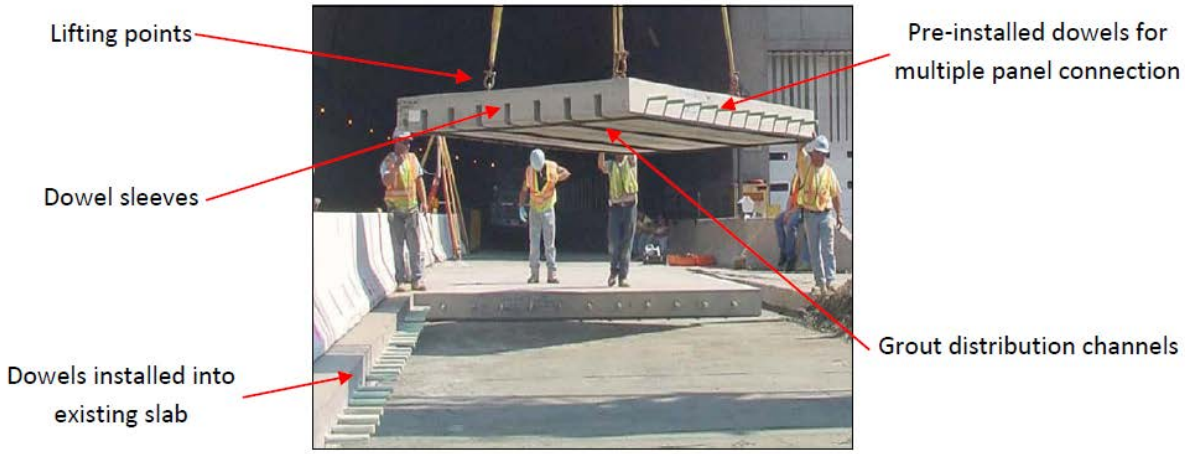

Figure 7. Grout Distribution Channels [3]

2.5.2. Michigan Method

The Michigan Method, developed by the Michigan Department of Transportation, is a non-proprietary method designed for single panel, full-depth repair of rigid highway pavements [4].

2.5.2.1. Load Transfer

Load transfer is accomplished by casting dowel rods into the precast concrete panel. There are three dowel rods in each wheel path, spaced 1 foot apart, which fit into dowel slots cut out of the existing slab. Figure 8 illustrates the load transfer dowel rods in the precast panel and the dowel slots in the existing PCC surface.

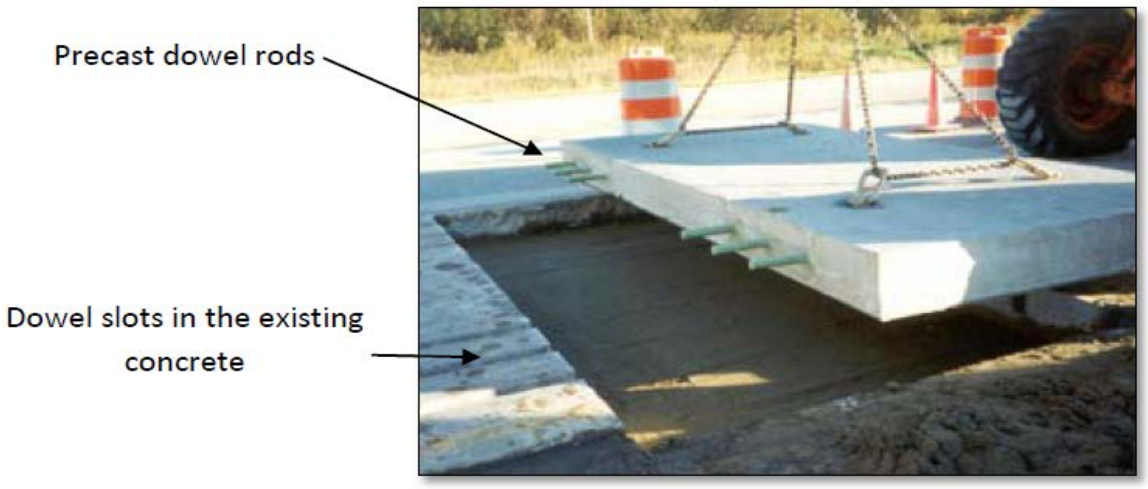

Figure 8. Load Transfer Dowel Rods and Dowel Slots, Michigan Method [4]

2.5.2.2. Base Preparation

The Michigan method incorporates a self-leveling, cementitious flowable fill (Figure 9). The flowable fill is typically placed above a well-compacted base course to ensure complete panel seating and leveling. Flowable fill is comprised of Portland cement, fly ash aggregate, fine mineral aggregate, ½- inch minus coarse mineral aggregate, and water.

Figure 9. Flowable Fill Placement [4]

2.5.3. Uretek Method

The Uretek method is a proprietary precast concrete panel repair process, used for single or multiple repairs.

2.5.3.1. Load Transfer

The Uretek method utilizes specially manufactured fiberglass ties (Figure 10) to serve as load transfer mechanisms [5]. The fiberglass ties are installed after placement of the precast panel. The ties are inserted and grouted into slots that extend from the existing slab to the precast concrete panel. Figure 11shows the Uretek fiberglass tie installation procedure.

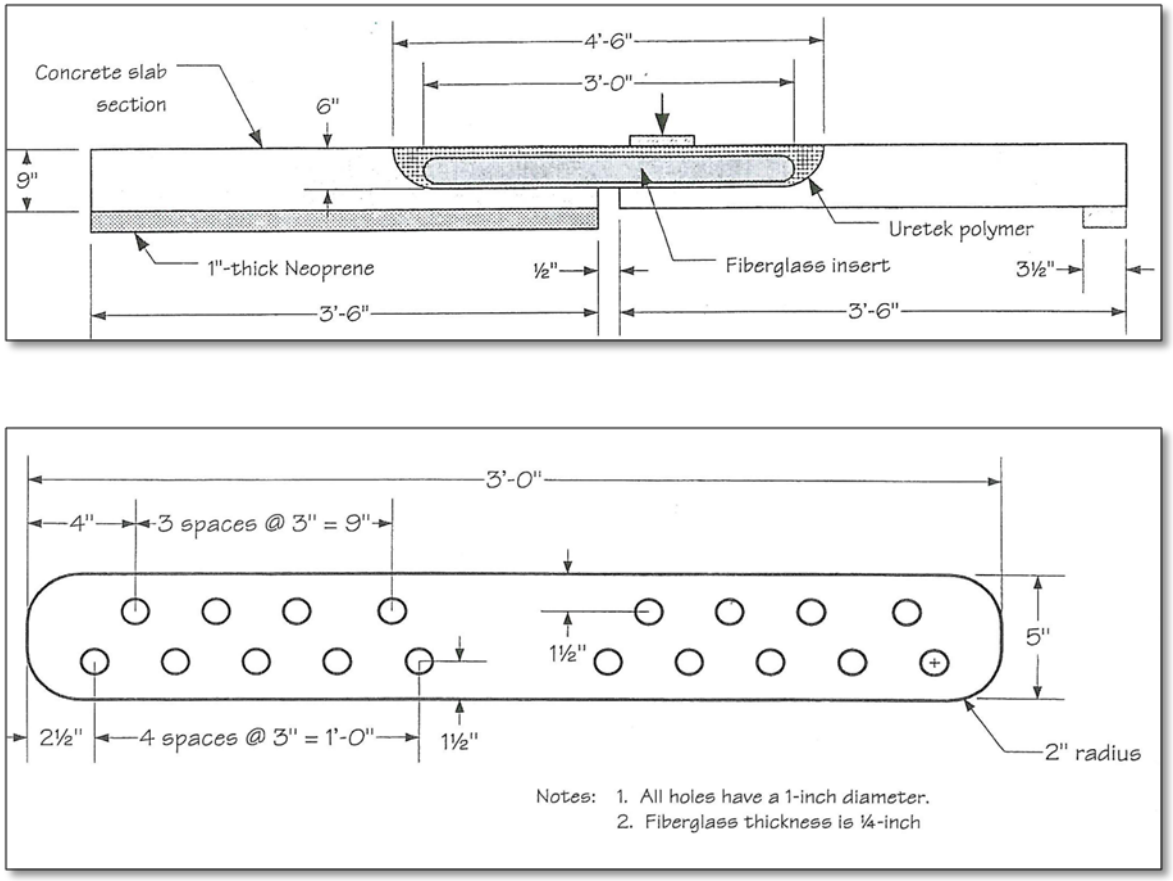

Figure 10. Uretek Fiberglass Tie Schematic [5]

Figure 11. Uretek Fiberglass Tie Installation Process [5]

2.5.3.2. Base Preparation

The distinguishing feature of the Uretek method technique for base preparation is the distribution of HDP foam, injected underneath the precast concrete panel after placement. The injection process, shown in Figure 12, utilizes several full-depth portholes to facilitate foam distribution.

The HDP foam is able to spread underneath the precast concrete panel while undergoing a chemical reaction causing it to both densify and expand. The foam exerts pressure on the underneath side of the precast panel forcing it to move in an upward direction. Multiple injection ports and precise leveling equipment ensure that the precast repair panel is even with the adjacent concrete slab. This base preparation method eliminates the precision grading required for the Fort Miller Super-Slab® and Michigan methods.

An alternative Uretek technique is a deep injection of the HDP foam. This process entails drilling portholes through the precast panel and several feet into the subgrade. The high density foam is then infused into the subgrade material, forcing the soil matrix to condense and forcing the precast panel upward.

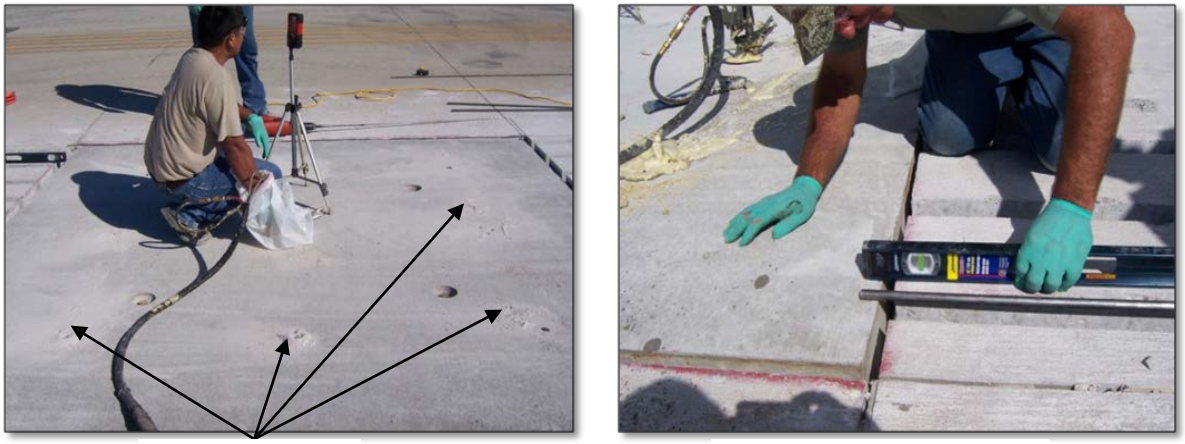

Injection ports

Leveling measurement

Figure 12. Uretek HDP Foam Injection Ports

2.6. Installation Procedures

The following section details precast concrete panel installation procedures. This section is designed to provide a general overview of the installation process, regardless of installation method.

2.6.1. Distressed Slab Removal

It is imperative that the full-depth repair encompasses the entire distressed portion of the existing slab. There are several methods that can be utilized for slab removal. The most common include the lift-out method and the shattering method. The lift-out method involves using a concrete saw to cut the distressed area into smaller, more manageable pieces. The shattering method entails hydraulically or pneumatically shattering the distressed area to facilitate removal. In some instances, if the damaged area is fairly localized, the entire perimeter of the repair area is cut away with a concrete saw and removed as a single unit. Templates are necessary to accurately mark the perimeter of the repair section. This helps to eliminate over-cutting or under-cutting the repair area.

Importantly, the designated repair area must be congruent to the precast concrete repair panel. Typically, the precast repair panels are designed to have a tolerance ⅛inch to ¼ inch lengthwise and widthwise. Precast panel thickness is generally ¼ inch to ⅝inches less than the existing slab. This eliminates the need to disturb the base course when placing new bedding material.

2.6.2. Precast Panel Size.

Facility owners should, if possible, limit the number of precast panel sizes. This streamlines the installation process and reduces costs. This may be difficult at facilities where concrete thickness varies considerably. In these instances, it may be necessary to custom-build precast concrete panels to fit the existing areas to be repaired.

2.6.3. Materials for Precast Concrete Panels.

PCC used in the construction of precast concrete repair panels should meet the same material standards as the existing PCC at the repair site. Additionally, the precast concrete panels require steel reinforcement to mitigate panel damage during the transportation and installation phases.

3. AFRL PRECAST CONCRETE PANEL REPAIR

Air Force Research Laboratory (AFRL) installed three precast concrete panels on the Aircraft Operating Surface (AOS) test-pad. The test pad consisted of 12 inches thick PCC. Each precast concrete repair panel was 11 inches in thickness and contained steel reinforcement to prevent damage during the transportation and installation operations.

Following installation, each of the repair slabs was subjected to accelerated traffic loadings using the F-15 load cart in a series of 1,508 passes. Before, during, and after the accelerated loading process, a HWD was utilized to measure load transfer between the parent slabs and the precast concrete repair slabs.

The following sections of this report detail the installation procedure for each of the three precast concrete panels. The major delineation between the three installations was the base course preparation method. Precast Panel 1 was leveled and supported by Uretek polyurethane foam injected directly underneath the slab. Precast Panel 2 was leveled and supported by Uretek polyurethane foam, injected 3 feet into the subgrade material. Precast Panel 3 was leveled and supported with a cementitious flowable fill, similar to the Michigan method. Each precast panel incorporated load transfer dowel rods installed prior to concrete placement, also similar to the Michigan method. Dowel slots were cut into the existing concrete to accommodate the load transfer dowel rods. The relative location of each precast concrete repair panel is illustrated in Figure 13.

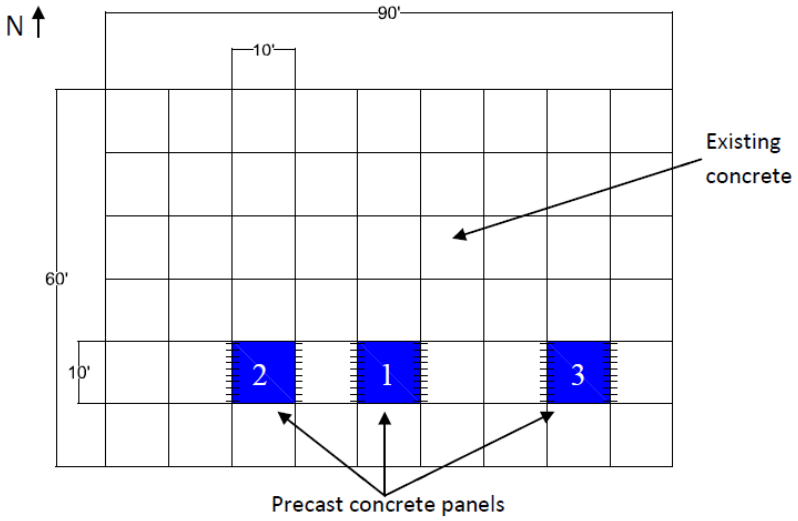

Figure 13. Precast Concrete Panel Repair Locations

3.1. Precast Panel 1

This section details the installation process for precast Panel 1. This panel incorporated pre-installed load-transfer dowel rods and was leveled and supported with Uretek HDP foam injected directly beneath the precast panel after placement.

3.1.1. Precast Panel Fabrication.

AFRL designed and constructed a steel form to manufacture precast concrete repair slabs. The form was a rigid steel frame measuring 9 feet 10 ½ inches by 9 feet 10 ½ inches. These specific dimensions guaranteed a ¾-inch construction joint between each edge of the precast concrete panel and the existing PCC slab. The frame could accommodate precast panels up to 12 inches thick and contained longitudinal dowel slots at both ends, allowing load transfer dowel rods to be pre-installed prior to fresh concrete placement.

Before concrete placement, it was necessary to ensure the steel frame was properly aligned and squared. After manipulating the frame into the proper position, several anchor bolts were inserted through tabs on the bottom of the steel frame and drilled into the existing concrete slab (Figure 14) to guarantee the frame maintained its position during concrete placement.

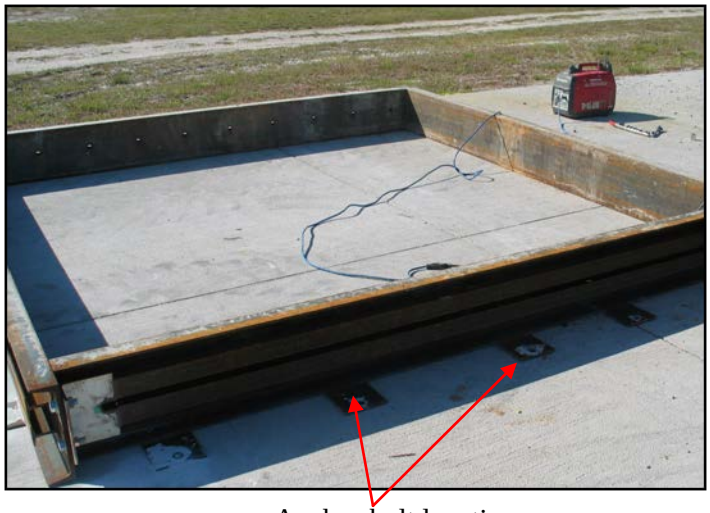

Figure 14. AFRL Precast Concrete Panel Form

After positioning the frame, a 1 inch thick layer of plywood was inserted in the form. The purpose of the plywood was to change the height of the frame from 12 inches to 11 inches. Subsequent to plywood placement, a steel reinforcement grid was constructed to mitigate concrete cracking concerns attributable to transportation and placement of the precast panel. The reinforcement grid consisted of ⅜ inch diameter rebar (#3) arranged in a 1 foot by 1 foot square pattern. A ⅜ inch concrete cover was maintained between the ends of the reinforcement bar and the side of the frame. The entire grid was placed on 1 ½ inch rebar stands, providing a rebar depth of 9 ½ inches from the top surface of the precast panel.

One inch diameter load transfer dowel rods were installed into the form before placement. The frame was designed with dowel openings, centered 5 ½ inches from the top surface, to allow the rods to be installed into the precast panel. Each 1 inch diameter dowel rod was 22 inches long. This length allocated 11 inches for the precast panel, with an additional 11 inches remaining to tie into the future slab. Dowel rods were spaced 1 foot apart, with the first dowel rod situated 6 inches from the edge of the existing PCC slab. Exterior dowel alignment forms ensured the dowel rods maintained the proper alignment during concrete placement (Figure 15).

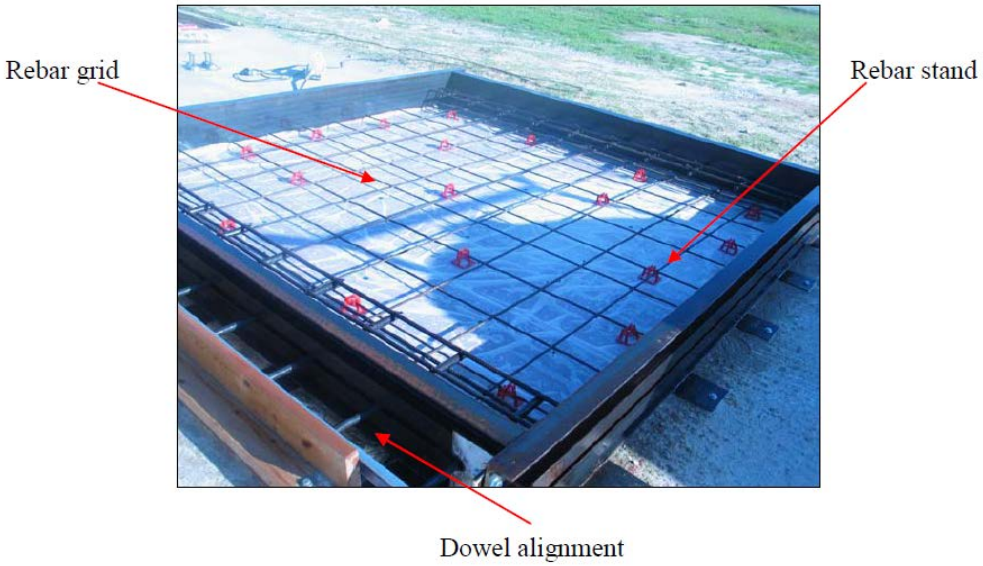

Figure 15. Precast Concrete Panel Dowel Alignment and Rebar Grid Configuration

3.1.1.1. Concrete Placement

Precast Panel 1 was constructed from concrete with a specified 28-day compressive strength of 5,000 psi. After placement, the concrete was vibrated into place and the surface initially finished with a bull float. Four 8,000 pound capacity swift-lift attachments, inserted 3 feet from each corner, were wet-set in the fresh, finished concrete to provide lifting points for the precast panel (Figure 16). A magnesium hand float was subsequently used to re-finish the areas disturbed during the swift-lift installation and a broom finish was applied for surface texturing.

Swift-lift attachments | Wet-setting swift-lift attachments | Installed swift-lifting points

Figure 16. Swift-Lift Installation into Precast Concrete Panel

3.1.2. Distressed Slab Removal

The 10-feet by 10-feet section of existing slab designated for removal was located and identified. The concrete cut-out was performed with a wall saw, which operated on a rail system. The rail was aligned along the marked perimeter of the cut-out section, which ensured straight, accurate cuts. The proper cutting procedure involved a series of passes, each pass increasing the total

depth of cut by one third of the total slab thickness. In this case, because the slab was 12 inches thick, each pass increased the depth of cut by approximately 4 inches. The cut was performed along the perimeter of the marked area, and each corner was cross-cut by one half of the saw-blade diameter. The wall-saw cutting operation is shown in Figure 17.

Figure 17. Wall-Saw Cutting Operation

After performing the cutting procedure along each edge, four 8,000 pound capacity swift-lift attachments were installed in the distressed slab. The lifting points were located 3 feet from each corner, the same configuration as the precast panel. To install the lifting attachments, four 6-inch-diameter full-depth cores were removed from the cutout section. Each core was extracted and the cored area cleared of debris and water. Pavemend 15.0™, a rapid-setting cementitious grout, was placed in the cored area. Then lifting attachments were wet-set in the freshly placed grout. The process is illustrated in Figure 18.

Mixing Pavemend 15.0™

Placing Pavemend 15.0™

Installing lifting attachment

Figure 18. Swift-Lift Installation into Existing Concrete

Pavemend 15.0™ set times are temperature dependent. As the name implies, final set typically occurs within 15 minutes after mixing. The set times vary based on the ambient temperature and the temperature of the water used for mixing the material. According to the manufacturer, the material may be mixed and placed in temperature conditions ranging from 30 °F to 120 °F, and the optimal water temperature is between 65 °F and 75 °F. Previous experience had demonstrated measurably increased set times in cool conditions, particularly when the mixing

water was colder than 50 °F. Experience had also shown that warmer ambient and water temperatures measurably decreased the set time of the Pavemend 15.0™ rapid-setting grout. Technical literature, provided by the Pavemend 15.0™ manufacturer, states that compressive strengths in excess of 2,500 psi are possible in 2 hours after placement. The minimum PCC compressive strength required for load applications involving the swift-lift attachment points is 1,800 psi [6]. Therefore, embedded lifting points were allowed to set in the Pavemend 15.0™ for at least 2 hours before lifting the slab.

The culmination of the slab removal process was the extraction of the distressed slab from the adjacent PCC matrix. A mobile crane was utilized to perform the lifting operations. Lifting attachment hardware was attached to each of the embedded swift-lift anchors. After properly connecting and securing the lifting hardware, the crane raised and removed the distressed slab (Figure 19).

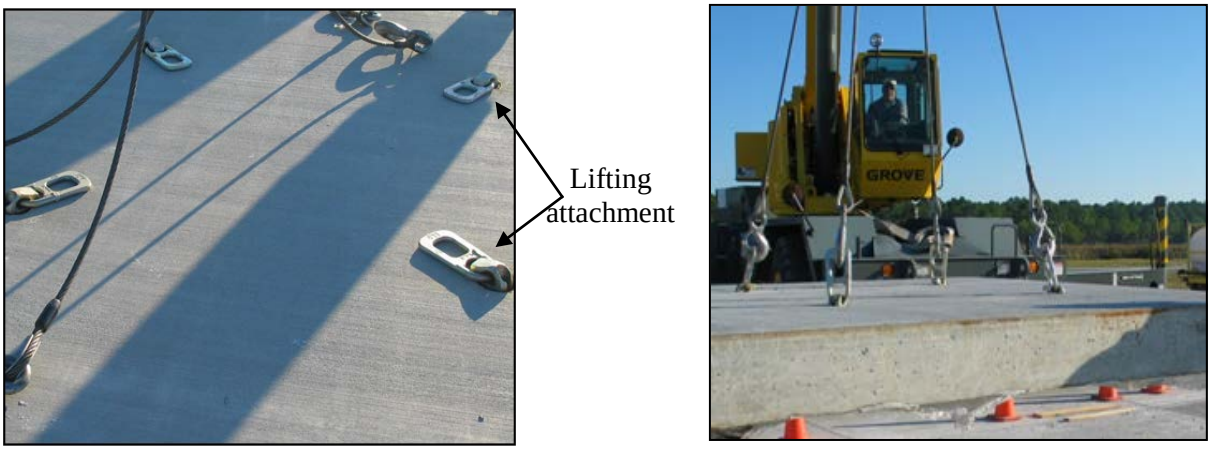

Figure 19. Distressed Slab Removal

Dowel slots, constructed to provide a receptacle for the load transfer dowel rods, were installed in the existing PCC slab after extracting the distressed slab. Each dowel receptacle measured 6 ½ inches deep, 2 ½ inches wide, and 24 inches long.

A dowel alignment template was constructed to ensure accurate cutting of the dowel slots in the existing PCC slab. After marking the dowel slots, a walk-behind concrete saw was utilized to perform the cutting operation. The walk-behind concrete saw cut the perimeter portion of the dowel slot, and a jackhammer was used to chisel and remove the inner portion of the slot. The process is exhibited in Figure 20.

The dowel slot construction procedure was subsequently modified to include excavation of the slots prior to removal of the distressed slab. This prohibited the saw operator from performing cutting operations over the void created by removal of the distressed slab.

Figure 20. Dowel Slot Construction in the Existing PCC Slab

3.1.3. Base Preparation

The primary objective of the AFRL precast concrete panel project was to determine the effect of different base preparation methods on the load transfer performance of the precast slabs. Three different precast concrete panels were each installed in different base conditions. Precast Panel 1 was leveled and supported by Uretek HDP foam, injected directly underneath the slab.

Each precast concrete panel was 11 inches thick. However, the existing PCC slab was 12 inches thick. In addition, 4 inches of the existing base course was excavated after the distressed slab was removed. This created a 16 inch gap from the base course to the PCC surface, which was partially filled with a new 4 inch thick well-compacted crushed-aggregate base course layer. The new base course layer was constructed to mitigate settling beneath the precast panel.

After constructing the new base course layer, a 12 inch gap still existed between the top of the base course and the PCC surface. This gap was designed to allow for a 1 inch height differential to remain between the surface of the existing slab and the surface of the precast panel. After placement of the precast concrete panel, Uretek HDP foam, pumped directly under the precast slab, was utilized to raise the precast panel the additional 1 inch and create a level surface with the adjacent PCC.

3.1.3.1. Panel Placement

Precast Panel 1 was transported from the construction site to the repair location. To facilitate transportation, a mobile crane and a flat-bed transportation vehicle were employed. The crane lifted precast Panel 1 with rigging hardware connected to the pre-installed swift-lift attachment points. After lifting, the precast panel was placed on the flat-bed transportation vehicle and driven to the repair location. Figure 21illustrates the panel lifting process.

Figure 21. Precast Concrete Panel Lifting Process

Crane rigging was reattached to the precast panel at the repair site to facilitate removing the panel from the transport vehicle. Guide-lines, attached to the panel during the lifting process, assisted personnel in manipulating the panel into the proper orientation. Additionally, ¾-inch-thick plywood spacers were placed in each corner of the excavated region. The spacers maintained the ¾-inch construction joint between the precast concrete panel and the existing slab, as well as protecting the corners of the precast slab. The installation process is shown in Figure 22.

Figure 22. Precast Concrete Panel Placement Process

3.1.3.2. Uretek HDP Foam Injection

Precast Panel 1 was leveled and supported with the Uretek polyurethane, high-density expanding foam, injected directly underneath the panel through portholes drilled after panel placement. Before injecting the foam, survey measurements were taken from each corner of the precast concrete panel to determine the pre-injection height differential between the PCC surface and the precast concrete panel surface. The results were as follows:

a) Southwest corner: 1 inch below PCC surface
b) Northwest corner: ⅝ inch below PCC surface
c) Northeast corner: 1 inch below PCC surface
d) Southeast corner: 1¼ inch below PCC surface

A total of nine ¾ inch diameter injection ports were drilled through the precast concrete panel after it was placed. The porthole configuration is illustrated in Figure 23. Subsequently, precision laser-leveling equipment was tactically placed near each corner of the precast concrete panel to allow test personnel to monitor the progress of the panel-jacking procedure in order to determine when each corner of the precast panel was level with the adjacent PCC slab.

Prior to beginning the panel-jacking operation, Uretek HDP foam was injected along the bottom perimeter of the precast concrete panel. The purpose was to create a seal, designed to keep the foam from blowing out of the sides during the injection operation (Figure 24). Injection operations commenced after achieving an adequate seal and were terminated when each corner of the precast panel was precisely level with the surrounding concrete slab. The injection operation is exhibited in Figure 24.

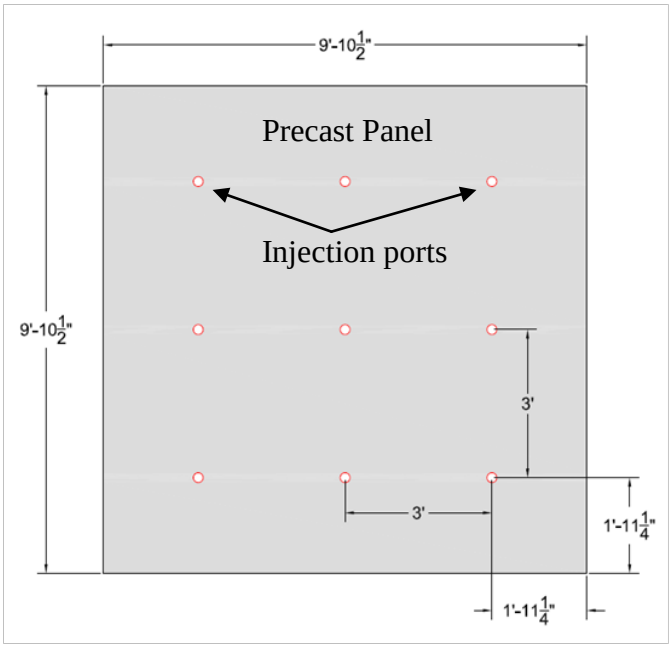

Figure 23. Uretek Direct Injection Porthole Layout

1) 

Porthole drilling operation and foam injection in the bottom perimeter of panel

2) 

Multiple foam injections

3 

Strategic foam injection

4) 

Precision leveling equipment

Figure 24. Uretek Direct Injection Procedures

3.1.4. Joint Sealant

The final installation procedure entailed joint sealing. The ¾ inch construction joint between the precast panel and the adjacent PCC slab was filled with Pavemend 15.0™. Pavemend 15.0™ was placed along each edge of the panel until the joints and dowel slots were completely filled. Hand tools were utilized to finish and brush the freshly placed grout. Lifting-point recesses and injection portholes were left un-grouted.

3.2. Precast Panel 2

The panel fabrication and installation procedures for precast Panel 2, including base course construction, were identical to the procedures detailed previously. The delineation between the panels was the panel-jacking/leveling method. Panel 2 was jacked/leveled with Uretek polyurethane foam, injected 3 feet into the subgrade material. The leveling procedure is detailed in the following section.

3.2.1. Uretek HDP Foam Deep Injection.

Survey measurements were taken at each corner of precast Panel 2 before commencing foam injection. The measurements detailed the height differential between the precast concrete panel and the adjacent PCC slab. The results were as follows:

a) Southwest corner: 1 inch below PCC surface
b) Northwest corner: 1 ⅜ inch below PCC surface
c) Northeast corner: ½ inch below PCC surface
d) Southeast corner: level with PCC surface

The porthole layout for Panel 2 was similar to the Panel 1 layout, except there were two injection ports separated by 2 inches at each location. One hole was a deep-injection port and the second hole was a shallow injection point. The shallow holes were identical to those previously described, designed to distribute Uretek HDP foam directly underneath the slab. In essence, the deep injection process performed a majority of the precast panel-jacking work, while the shallow injections allowed for precision leveling.

Deep porthole construction consisted of drilling a ¾ inch diameter shaft through the precast panel and 3 feet into the subgrade material. A ¾ inch diameter hollow metal rod was inserted into the drilled cavity to prevent collapse (Figure 25). Laser-sighting equipment, used to monitor the panel leveling progress, was placed in each corner of the precast panel prior to commencing the injection operations.

Deep injection operations were terminated in a particular region when the closest proximity precast-panel corner was raised to approximately ⅛ inch below the surface of the PCC slab. Shallow injection operations were then utilized to complete the slab-jacking procedure and ensure the precast panel was even with the existing slab. Subsequently, the joints and dowel slots were grouted with Pavemend 15.0™ .

Figure 25. Installation of Hollow Injection Rods for Uretek Deep Injection

3.3. Precast Panel 3

Precast Panel 3 maintained the same physical dimensions as precast Panels 1 and 2. However, Albright heat-resistant concrete was used in place of conventional PCC. Albright concrete, comprised of a proprietary mixture design, was originally designed to resist concrete degradation caused by the extreme temperatures emitted from the thrust forces of military aircraft. Albright concrete cylinders, tested in accordance with ASTM C 39 (Standard Test Method for

Compressive Strength of Cylindrical Concrete Specimens), achieved 28-day compressive strengths in excess of 6,000 psi.

Panel 3 installation process differed from Panels 1 and 2 in two aspects: 1) Distressed slab removal; 2) Base preparation. The following sections detail the distressed slab removal procedures and the base preparation method.

3.3.1. Distressed Slab Removal

The distressed section was demarcated from the surrounding slab and removed with a walk-behind concrete saw, as opposed to a wall saw. The walk-behind concrete saw expedited the slab-cutting process considerably. However, the walk-behind saw required a skilled operator to perform straight, accurate cuts.

The walk-behind saw-cutting procedure was similar to that of the wall saw cutting procedure. A series of three passes was utilized to perform a full-depth cut. Each pass increased the depth of cut by 4 inches, which was a third of the PCC slab thickness. Lifting anchors were installed in the distressed slab after cutting, to facilitate extraction.

3.3.2. Base Preparation (Flowable Fill)

A new base course layer was constructed after removing the distressed slab. The base course layer construction method was the same as previously described. A 12-inch gap remained between the top of the base course and the surface of the PCC slab. This gap allowed for a 1-inch-thick flowable fill layer to support precast concrete Panel 3.

The flowable fill mixture was designed by a local ready-mix plant. It was comprised of Portland cement, fly ash, fine mineral aggregate, and water. The material was transported from the plant using a ready mix concrete truck and placed on site.

Precast Panel 3 was positioned near the repair location in order to facilitate an expedited panel installation. The expedited installation was required to guarantee the flowable fill did not set before placement of the precast panel. It was assumed that the fill would compress. Therefore, a 1 ½ inch thick layer of the material was placed in the excavated section, which allowed for a 10 ½ inch gap between freshly placed flowable fill and the surface of the PCC slab.

Immediately following placement of the fill, precast concrete Panel 3 was installed. However, the flowable fill did not compress an adequate distance and the precast panel surface came to rest approximately ¼ inch higher than the adjacent PCC surface. The incompressibility of the material was possibly attributable to the fact that the fill was surrounded by the PCC slab, except underneath. This created a relatively impermeable environment.

The ¼ inch height differential between the PCC slab and the precast concrete panel was not acceptable. Consequently, precast Panel 3, still attached to the crane, was removed. The freshly placed flowable fill, and a 6-inch-thick layer of the newly constructed base course, were subsequently excavated from the repair location.

After excavation, a new base course layer was constructed in the same location. The new base course layer was 3 inches thick. This arrangement required a 4 ½ inch thick flowable fill layer, but ensured that the bottom 3 inches of the layer would be surrounded by soil. A 10 ½ inch gap remained between the flowable fill and the PCC surface. Figure 26shows the first and second installation configurations.

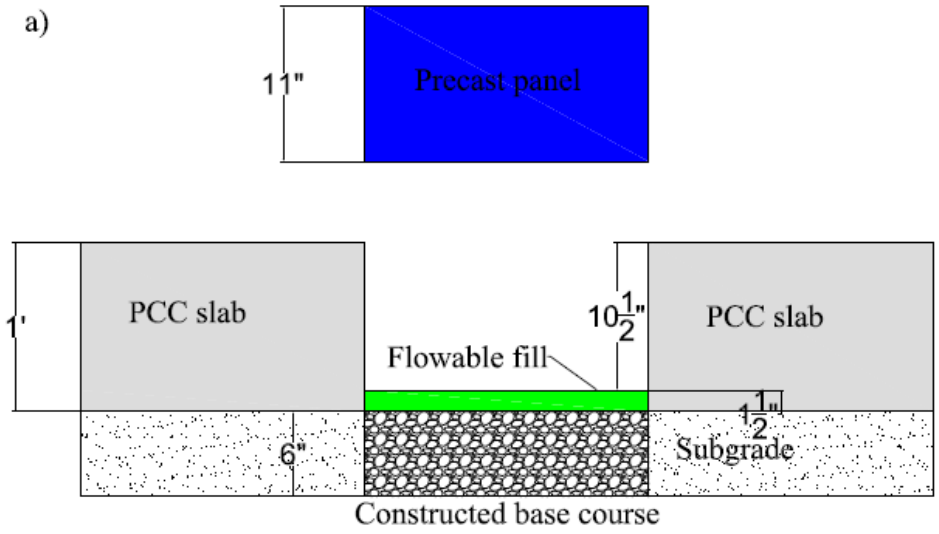

First, Unsuccessful, Precast Panel 3 Base Course Preparation Configuration

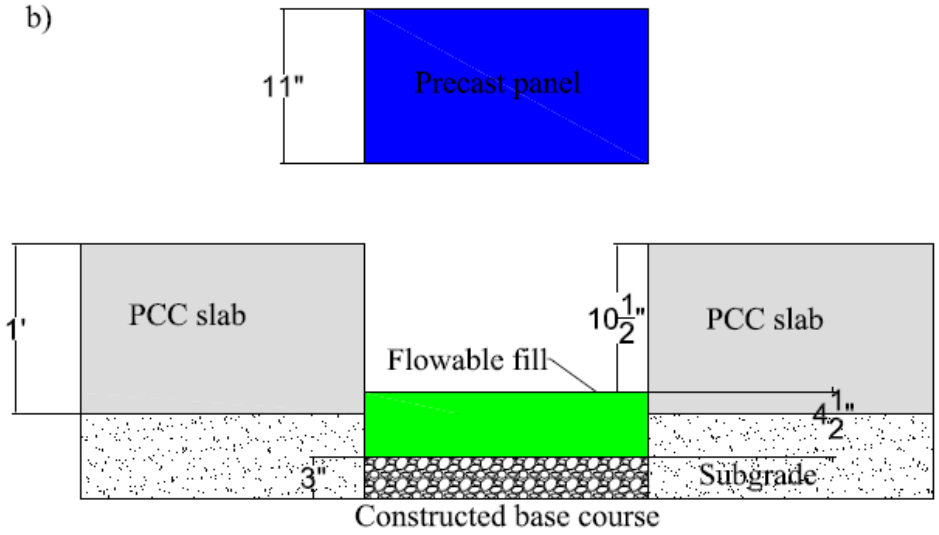

Second, Successful, Precast Panel 3 Base Course Preparation Configuration

Figure 26. First and Second Precast Panel 3 Base Course Preparation Configurations

Immediately after placement of the flowable fill, precast Panel 3 was re-installed in the repair location. Due to concerns that the panel might sink into the flowable fill, each panel corner was

equipped with a steel plate. The plates were mechanically connected to the top surface of the precast panel, and oriented so that a portion overhung each side of the panel's corner, bridging the surfaces of the precast panel and the adjacent PCC. The second installation of precast panel 3 was successful. The 4 ½ inches of fill material compressed an adequate amount to accommodate the full-depth of the replacement slab. Following installation, rapid-setting grout was used to seal the joints and dowel slots as described above.

3.4. Installation Timeline

The following section details the installation timeline for each of the three precast panel repair operations. Additionally, precast panel fabrication and precast panel placement timelines have been provided. The timeline data was compiled during the precast concrete panel installation and construction phases of this project.

Table 1, Table 2, and Table 3 are installation timelines for Precast Panels 1, 2, and 3, respectively. Table 4 and Table 5 are timelines for distressed slab removal operations (Wall-saw and walk-behind concrete saw). Table 6 is a precast concrete panel fabrication timeline and Table 7 is precast panel placement timeline.

Table 1. Precast Concrete Panel 1, Uretek Direct Injection Timeline

Task	Time (minutes)
Dowel slot cutting/removal (existing PCC slab)	60
Base course excavation	60
Base course construction	60
Precast panel placement	15
Porthole drilling operations	45
Uretek injection and leveling operations	60
Placement of joint and dowel fill material	30
Rapid-set finishing	5
Total	335

Table 2. Precast Concrete Panel 2, Uretek Deep Injection Timeline

Task	Time (minutes)
Dowel slot excavation (existing PCC slab)	60
Base course excavation	60
Base course construction	60
Precast panel placement	15
Porthole drilling operations	90
Uretek injection and leveling operations	60
Placement of joint and dowel sealant	30
Rapid-set finishing	5
Total	380

Table 3. Precast Concrete Panel 3, Flowable Fill Timeline

Task	Time (minutes)
Dowel slot excavation (existing PCC slab)	60
Base course excavation	60
Base course construction	60
Flowable fill placement (simultaneous with slab install)	20
Precast panel placement	15
Placement of joint and dowel sealant	30
Rapid-set finishing	5
Total	250

Table 4. Distressed Slab Removal with Wall-Saw Timeline

Task	Time (minutes)
Mark perimeter of distressed slab	20
Saw-cutting operations	240 (four sides @ 60 minutes each)
6-inch-diameter coring operations	20 (four cores @ 5 minutes each)
Rapid-set mix and placement	10 (four cores @ 2.5 minutes each)
Swift lift installation	5 (four anchors)
Rapid-set cure time	15 (Temp/weather dependant)
Attach crane rigging hardware	5
Extract distressed slab	10
Total	325

Table 5. Distressed Slab Removal with Walk-Behind Concrete Saw Timeline

Task	Time (minutes)
Mark perimeter of distressed slab	20
Saw-cutting operations	80 (four sides @ 20 minutes each)
6-inch-diameter coring operations	20 (four cores @ 5 minutes each)
Rapid-set mix and placement	10 (four cores @ 2.5 minutes each)
Swift lift installation	5 (four anchors)
Rapid-set cure time	15 (Temp/weather dependant)
Attach crane rigging hardware	5
Extract distressed slab	10
Total	165

Table 6. Precast Concrete Panel Fabrication Timeline

Task	Time (minutes)
Form set-up	240
Rebar cutting operation	20
Rebar mat fabrication	60
Dowel rod placement and alignment	60
Concrete placement	10
Concrete finishing	45
Swift-lift insertion	5 (four anchors)
Total	440

Table 7. Precast Concrete Panel Placement Timeline

Task	Time (minutes)
Attach rigging hardware	5
Lifting operation (from constructed site to truck)	15
Lifting operation (from truck to repair area)	15
Total	35

3.4.1. Optimal Precast Panel Installation Procedures

The following sections detail the optimal methods for distressed slab removal, precast panel fabrication, precast panel placement, and precast panel base preparation. The results are based the time required to complete each task, and the feasibility and efficiency of each method.

3.4.1.1. Distressed Slab Removal

The walk-behind concrete saw is recommended to cut the damaged PCC section away from the surrounding PCC slab. Utilizing the walk-behind saw reduced the slab cutting process from 325 minutes (wall-saw operation) to 165 minutes (walk-behind saw operation). This was a substantial improvement and clearly illustrated the operational utility and advantage of this piece of equipment. However, the necessity of an experienced operator is a major drawback to utilizing the walk-behind saw. Airfield damage repair (ADR) teams will need to incorporate a skilled saw operator in order to take advantage of the walk-behind concrete saw to complete repairs in the most expeditious timeline possible.

Also, dowel slots should be constructed in the existing pavement prior to removal of the distressed slab. This eliminates the need for the walk-behind concrete saw operator to perform cutting operations over the void created by removal of the slab, which is clearly a hazard to the operator and test personnel in the vicinity of the repair.

3.4.1.2. Precast Panel Fabrication

A rigid precast panel form is required to ensure the freshly placed concrete maintains its proper dimensions during placement. An adjustable rigid form may be advantageous in scenarios which will require repair panels of variable dimensions. It is imperative that the rigid panel form

incorporate a dowel alignment tool to maintain the proper orientation of the load transfer dowel rods during concrete placement.

Additionally, steel reinforcement is required to mitigate the precast panel from cracking issues during the transportation and placement operations. Electric hand-held band saws, used for rebar cutting operations, are essential to maintain the rebar cutting timeline outlined in Table 6.

3.4.1.3. Precast Panel Placement

Swift lift attachments provide a lifting point on the precast panel. These lifting attachments may be wet-set in the freshly placed concrete or attached in place on the form prior to placement. Pre-placement of the lifting attachments increases the installation time by 10 to 15 minutes. If wet-setting, it is important to allow the fresh concrete to set for several minutes prior to inserting the lifting points. If the fresh concrete has not had sufficient time to set, the removable rubber inserts may cause the lifting points to float higher than the freshly placed PCC.

An appropriately rated crane is required to lift each precast panel. Crane rigging should remain attached to the precast panel after lifting the panel from its storage site to the transportation vehicle to eliminate the necessity of reattaching the rigging hardware to the precast panel for placement in the repair area. When possible, situate the precast concrete repair panels in close proximity to the repair area to reduce transportation times.

L-shaped plywood spacers are required in at least two corners of the repair area to guarantee a congruent construction joint on all four sides between the precast panel and the existing slab. Failure to insert these spacers increases the installation time and creates a risk to the corners of the precast panel.

3.4.1.4. Base Preparation

Based strictly on the installation timelines, flowable fill is the most attractive base preparation method. However, as discussed subsequently in Sections 4 and 5, Uretek HDP foam (conventional and deep injection methods) significantly outperformed flowable fill in measures of LTE. Also, as illustrated in Section 3.3.2, it is difficult to pre-determine the requisite volume of flowable fill necessary for base preparation; which can negatively impact the installation procedure and substantially increase the installation timeline.

The HDP injection base preparation methods demanded similar installation times. The conventional injection operation took 335 minutes, as opposed to 380 minutes for the deep injection operation. The abbreviated conventional installation was due to the fact that the deep injection operation incorporated 9 additional injection ports and required the insertion of 9 deep-injection, hollow HDP transport tubes.

HDP installation times, conventional and deep injection, are expected to decrease significantly with repetition. It is likely that the disparity between the two HDP injection methods will also decrease, and the deep injection timeline will approach the conventional installation timeline.

4. PERFORMANCE EVALUATION OF THE REPAIRED SECTIONS

4.1. Background

Load transfer is a fundamental parameter in the mechanistic analysis and design of repaired pre-cast panels. Figure 27 shows the load transfer mechanism in rigid pavements. Load transfer is essentially a design parameter that characterizes the reduction in the stresses and strains in the loaded slab due to presence of load transfer devices at the joint. Load transfer depends on environmental conditions such humidity and temperature as well as stiffness of the base, moisture content, drainage system, joint spacing, load transfer devices such as dowel rods, construction quality, installation technique, magnitude of the wheel load and number of load applications [7]. Figure 27 shows the maximum plastic deformation at the joint for loaded slab $(\varepsilon_p)_l$ and unloaded slab $(\varepsilon_p)_{ul}$.

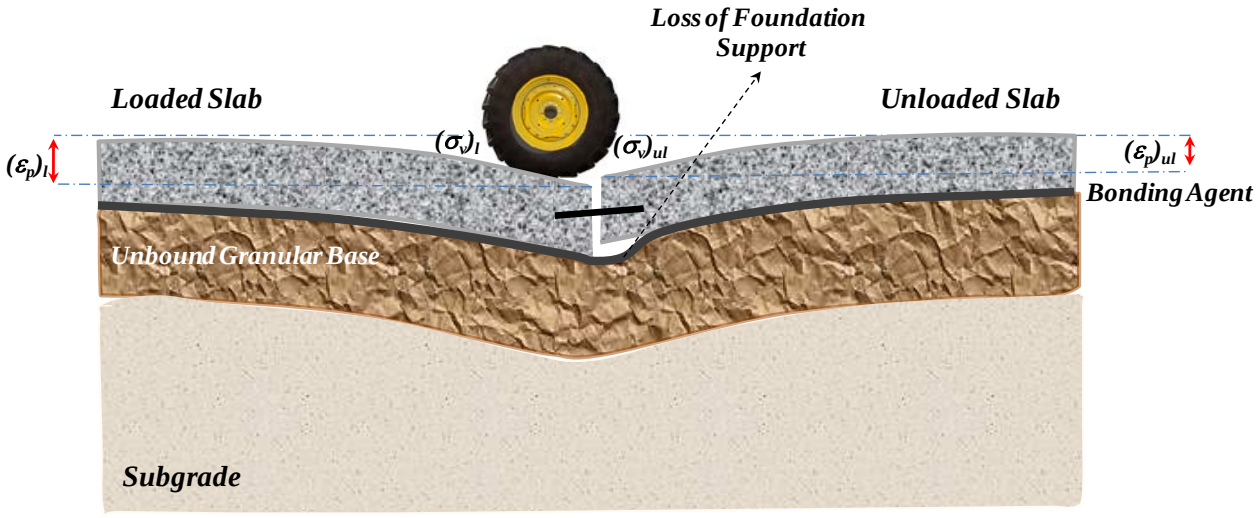

Figure 27. Load Transfer Mechanism in Rigid Pavements

This figure also shows the maximum vertical stresses at the loaded slab $(\sigma_v)_u$ and at the unloaded slab $(\sigma_v)_{ul}$. Pavement responses at the joint are typically used to characterize the efficiency of load transfer devices and installation techniques.

This section presents the experiment design factorial used to develop an efficient and effective protocol for installation of pre-cast repair panels. Field performance of the repaired sections was evaluated using an HWD. The weight of the impact load in the falling weight deflectometer (FWD) device was selected to simulate the aircraft load and to induce stresses and strains within the range of responses in airfield runways.

HWD testing was used to measure the plastic deformations imposed by the drop weight under the loading and unloading slabs. This data was in turn used to determine the trends of LTE, joint

stiffness and deformation energy dissipated to the slab foundation for each permutation of the experiment design. This section also describes the performance characterization of repaired sections using accelerated field loading to study the impact of load repetition on the loss of LTE and the decay of joint stiffness.

4.2. Experiment Design Variants

Table 8 presents the permutations of the experiment design in this study. Three installation techniques and two bonding agents were used to install the pre-cast panels. The position of the loading frame and the direction of loading were also indicated in this table. This information is used to assess the directional dependency of the LTE at the joints of pre-cast panels and pre-existing concrete slabs.

HDP and flowable fill were used as bonding agents and leveling materials for installation of precast panels. The main role assumed for the bonding agents was to provide proper adhesion between the pre-cast slab and the foundation to eliminate residual shear stresses created due to slippage. Bonding agents also act as leveling materials in the installation process of the repaired panels. In this study, pre-cast slabs were installed using conventional leveling techniques and deep injection methods. More information on the installation techniques and leveling materials are presented in Sections 2 and 3.

Table 8. Variants of the Experiment Design

Variant	*Pre-cast Panel No.*	*Joint Orientation*	*Bonding Agent*	*Installation Method*	*HWD Direction*
1	#1	East	HDP Foam	Direct Injection	East to West
2	#1	West	HDP Foam	Direct Injection	East to West
3	#2	East	HDP Foam	Deep Injection	East to West
4	#2	West	HDP Foam	Deep Injection	East to West
5	#3	East	Flowable Fill	Conventional	West to East
6	#3	West	Flowable Fill	Conventional	West to East
7	#3	East	Flowable Fill	Conventional	East to West
8	#3	West	Flowable Fill	Conventional	East to West

4.3. Determination of Load Transfer and Joint Stiffness using HWD

An FWD is a non-destructive testing device used to evaluate the structural capacity of pavement layers. This device is widely used by highway engineers for selecting proper maintenance and rehabilitation strategies. The FWD loading system, with load magnitudes ranging from 1,500-27,000 lbf (7-120 kN), applies an impact force on the surface of the pavement. The magnitude of this load is selected to simulate the expected loading conditions in the field. An HWD with load levels ranging from 6,500-54,000 lbf (30-240 kN) is typically used to evaluate the structural capacity of airfield runways. Plastic deformations resulting from the drop of the load at two sides of the joint, at several radial distances, are measured by a series of geophone sensors. The recorded responses and layer thicknesses are in turn used to back-calculate the modulus values of each layer. This information can be used to mechanistically determine the structural capacity and

the effectiveness of the repair methods. Figure 28 shows a typical HWD used in airfield runways.

Figure 28. Heavy Weight Deflectometer (HWD)

Figure 29 schematically illustrates the deflection basin resulting from the impact load at two sides of the joint. As shown in this plot, the HWD load is applied at one side of the joint close to the edge of the slab and the deflections were measured under load, at several radial distances in the unloaded slab. The deflection sensors, geophones, were placed 12 inches apart. Due to the discontinuity in the continuum, the gradient of the deflection basin changes significantly at two sides of the slabs. Proper design and installation of load transfer devices will reduce the rate of change in gradient of the deflection basin. Larger differences between the slope of the deflection basin on the two sides of the joint is an indication of poor load transfer capability of the load transfer devices or loss of foundation support. On the other hand, rigid pavement with no discontinuity in the deflection basin on either side of the joint corresponds to ideal load transfer capability of the slab-foundation systems.

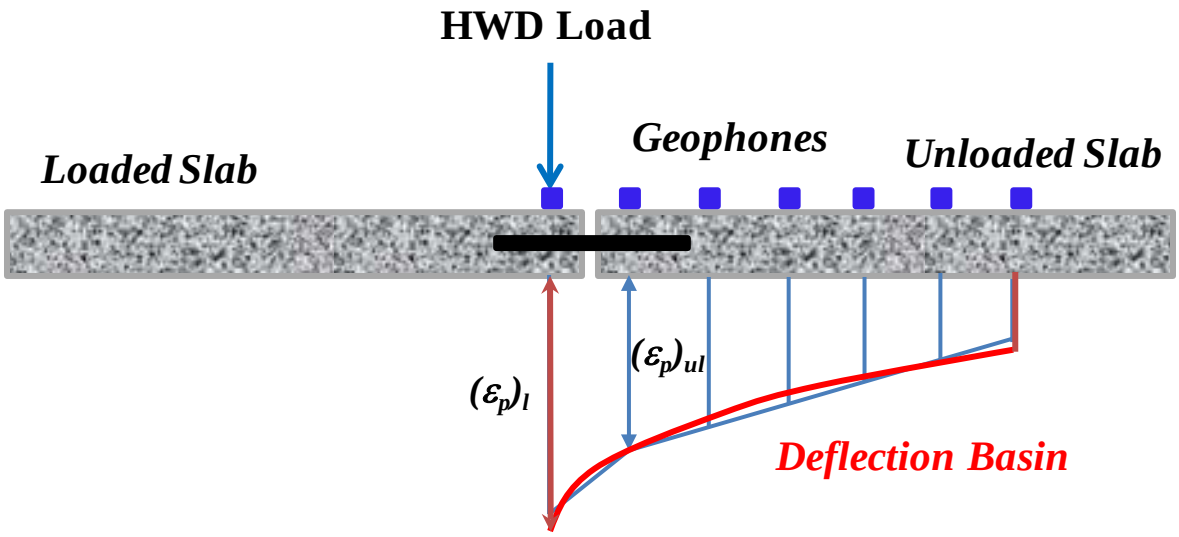

Figure 29. Deflection Basin Resulting from FWD Loading System

Figure 30 shows the placement of the HWD at the joint. This figure shows the impact load is located at the edge of the loaded slab at the right side of the picture and geophones were placed 12 inches apart on the unloaded slab. These measurements were in turn used to generate plots of deflection basin and tables of AREA.

Figure 30. Placement of HWD Loading Frame and Geophones at the Edge of the Slabs

4.4. AREA Concept

The AREA parameter was originally developed in early 1980s to analyze the deflection basin in rigid pavements. This parameter essentially combines the effect of all deflections measured by sensors when the repaired slab was subjected to HWD loading system. The AREA parameter is an informative analysis tool to quantify the effect of different construction techniques on the performance of the repaired sections. Equation 1 presents mathematical definition of AREA [8].

$$AREA = \frac{1}{2(\varepsilon_p)_o}\left[(\varepsilon_p)_o d_1 + \left[\sum_{i=1}^{n-1}(\varepsilon_p)_i (d_{i+1} - d_i)\right] + (\varepsilon_p)_n (d_n - d_{n-1})\right] \quad (1)$$

Where:

$(\varepsilon_p)_i$=plastic deformation measured at location i and (i=0,…,n)
n= number of geophones minus one
d_i= distance between the center of the load plate and geophones

It is important to note that the AREA parameter is not truly an area for it is normalized by maximum deflection which happens at the edge of the loaded slab. Therefore, AREA parameter has a dimension of length. The tables of AREA for each permutation of the experiment design are presented in Appendix A of this report.

4.5. Performance Degradation

Loss of LTE and decay of joint stiffness with number of load repetitions was also evaluated in this study. The deflections resulted from the application of HWD impact load after 0, 112, 256, 512, 752, 1008, 1248 and 1504 applications of the F-15 load cart were recorded. LTE, joint stiffness and deformation energy at each interval were calculated to monitor the effect of number of load applications on the performance degradation in the repaired sections. Figure 31 shows the load cart and loading channels of the pre-cast repaired panels. AFRL's F-15 loading cart carries 35,200 lbs on a single wheel, representing one-half of F-15's main loading gear, with approximately 315 psi tire pressure.

Figure 31. Accelerated Loading of the Repaired Sections Using F-15 Load Cart

5. LOAD TRANSFER EFFICIENCY (LTE)

When the aircraft passes over a joint in a concrete pavement, both approaching and departing slabs deform due to load transfer between the slabs. Load transfer mechanisms such as steel reinforcement (dowel rods), aggregate interlock, and foundation support result in distribution of the aircraft load between the PCC slabs at the joints. Therefore, pavement responses such as stresses and strains are significantly lower compared to situations where no load transfer device is present— such as slabs with free edge or in the vicinity of major cracks. Capability and efficiency of the load transfer devices to distribute aircraft loads acting on the departing slab to the surrounding slabs is an important design parameter which is quantified by LTE. LTE is a measure to determine the contribution of the approaching slab and the load transfer devices in reducing the stresses and strains in the loading slab.

There are several mechanistic approaches for determination of LTE. The rationale behind each criteria and the applicability of these measures to pre-cast damage repair panels is discussed in this section.

LTE based on plastic strains under the loaded and unloaded slabs, is the most common measure used to calculate LTE in the design of rigid pavements. Deflection based LTE (LTE_δ) is basically the ratio of maximum deflection at the joint of the loaded slab and the deflection of the unloaded slab measured across the joint as presented in Equation 2.

$$LTE_\delta = \frac{d_u}{d_l} \tag{2}$$

Where:

LTE_δ = deflection based LTE
d_u = plastic deformation under unloaded slab
d_l = plastic deformation under loaded slab

Layer deformation models and system deformation models are the two major permanent deformation approaches to characterize the permanent deformation behavior of pavement systems subjected to traffic loads. It is imperative to distinguish between the two concepts for the proper understanding of the LTE in repaired sections.

The layer deformation model estimates the non-recoverable strains (plastic deformations) in each finite layer as a function of the elastic strain in that layer and the material parameters for that layer. In other words, total deformation or the deformation at the top of the pavement is equal to the sum of plastic deformations calculated for each layer. Material parameters for each layer are determined in the laboratory using repeated load permanent deformation tests.

On the other hand, system deformation models treat the pavement as a whole and calculate the plastic deformation deposited in the continuum as total plastic deformation or deflection in the body of the material. System deformation models need only one set of permanent deformation parameters (model parameters) to characterize the deformation behavior of pavement systems.

The formulation of deflection based LTE presented in Equation 2 is based on the system deformation concept. The deformations measured by HWD geophones are regarded as total

deformation deposited in the pavement section regardless of the contribution of each layer to surface deflections.

If the repaired section shows poor ability to transfer aircraft load, the differential settlement [d_u-d_l] will be high and therefore LTE values are close to zero. On the other hand, for well performing joints, the pre-cast panels and pre-existing slabs act as one elastic rigid system and therefore the deflections at both sides of the joints are minimal. In this case, the magnitude of the LTE is close to one [9].

Equation 3 presents another formulation for deflection based LTE.

$$LTE_{\delta}^{*} = \frac{2d_u}{d_l + d_u} \tag{3}$$

The relationship between the two measures of deflection based LTE is presented in Equation 4.

$$LTE_{\delta}^{*} = 2\left[1 - \frac{1}{1+\frac{LTE_{\delta}}{100}}\right] \tag{4}$$

In the analysis of the pre-cast repair panels these two indices resulted in the same trend and ranking as expected. Therefore, LTE_{δ} is used for generating plots of deflection based LTE in this chapter and the analysis results based LTE_{δ}^{*} is reported in Appendix B. Comparisons between LTEs for individual slabs are presented in Appendix C.

Another method to calculate the load transfer efficiency in rigid pavements is based on the stresses under the PCC slabs at joints. Equation 5 presents the stress-based LTE.

$$LTE_{\sigma} = \frac{\sigma_u}{\sigma_l} \tag{5}$$

Where:

LTE_{σ}= stress based LTE
σ_u= stress at the joint of the unloaded slab
σ_l= stress at the joint of the loaded slab

Precast repair systems with higher LTE_{σ} and LTE_{δ} are expected to perform better in terms of lower differential settlements when subjected to aircraft loads. LTE_{σ} and LTE_{δ} range from zero corresponding to poor load transfer to one that corresponds to excellent load transfer between the repaired section and pre-existing slab.

Another criterion for LTE was designated by Federal Aviation Administration (FAA) based on the stresses in loading and unloading slabs. Equation 6 presents the relationship between FAA load transfer (LT) and LTE_{σ} [9].

$$LT = \frac{LTE_{\sigma}}{1+LTE_{\sigma}} \tag{6}$$

The cut off (or minimum) value for LT in FAA design guide is assumed to be 0.25. The accepted value of 0.25 was primarily based on the data collected and analyzed from test sections in mid

1940s to mid-1950s. LT ranges from zero for poor performing sections to 0.5 for ideal performing condition.

Relationship between Measures of Load Transfer Efficiency

In order to mechanistically derive the relationship between different measures of LTE, it is necessary to define a design parameter that relates material properties to the maximum allowable deflection under the PCC slab. This measure is called radius of relative stiffness (*l*) and can be calculated using Equation 7.

$$l = \sqrt[4]{\frac{E\,h^3}{12\,k\,(1-\upsilon^2)}} \tag{7}$$

Where:

l= radius of relative stiffness
E= modulus of PCC slab (psi)
h=thickness of PCC slab (in)
k=modulus of subgrade reaction (pci)
ν= Poisson ratio for PCC slab

The dimensionless parameter *(a/l)*, where *a* is the radius of the loaded area, was used by several researchers to characterize the deflection of concrete slab subjected to traffic loads. Equations 8 and 9 present Westergard's derivations of the corner deflections under the loaded and unloaded slabs respectively [10].

$$U_l = \frac{P}{kl}\left[1.1 - 0.8\sqrt{2}\left(\frac{a}{l}\right)\right] \tag{8}$$

$$U_u = 7.5\,log^{-1}[0.74\log f - 194] * \frac{1}{2}\left(\frac{a}{l}\right)^2 \tag{9}$$

Where:

U_l= corner deflection under loaded slab
U_u= corner deflection under unloaded slab
P= wheel load (lbs)
k=modulus of subgrade reaction (pci)
l= radius of relative stiffness
a= radius of loaded area (in)
f= joint stiffness

Figure 32 shows the sensitivity of the *(a/l)* parameter to the modulus of the PCC slab for different load radii. The general trend suggests that the *(a/l)* parameter reduces as the modulus of the slab increases. However, the curves tend to reach an asymptotic value with increasing values of PCC modulus. On the other hand, the radius of the loaded area is shown to significantly impact the gradient of the curves and therefore the sensitivity of the *(a/l)* parameter to PCC modulus. As illustrated in this figure, *(a/l)* is relatively insensitive to PCC modulus for small values of load print, while the sensitivity increases with increasing values of *a*. In this study, the radius of the loaded area by HWD was measured to be 5.9 inches.

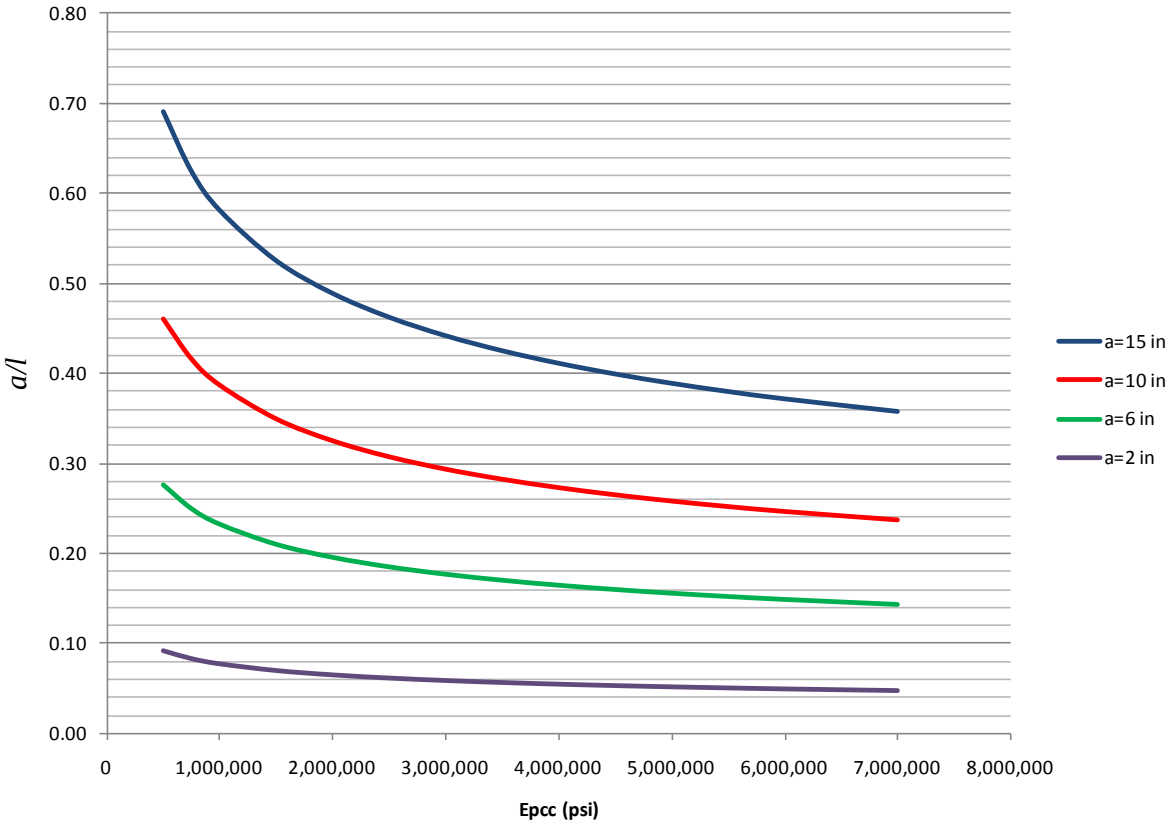

Figure 32. Variation of (a/l) Parameter with Respect to the Modulus of PCC Slab

Equation 10 presents the relationship between stress-based LTE and deflection based LTE developed by Ioannides and Hammons [11].

$$LTE_{\delta} = \frac{\left[1206\left(\frac{a}{l}\right)+377\right] LTE_{\sigma}^{2} - 393\left(\frac{a}{l}\right) LTE_{\sigma}^{3}}{1+698\left(\frac{a}{l}\right) LTE_{\sigma} + \left[370-154\left(\frac{a}{l}\right)\right] LTE_{\sigma}^{2}} \quad (10)$$

Figure 33 shows the sensitivity of the stress-based and deflection based LTE with respect to the load size ratio *(a/l)*. This plot indicates that the gradient of the LTE_{δ}-LTE_{σ} curves are higher when the load acts on a small area such as concentrated or point loads. However, larger load prints are shown to have lower sensitivity to the *(a/l)* value, which is in conformity with finite element analysis results by Korovesis [12].

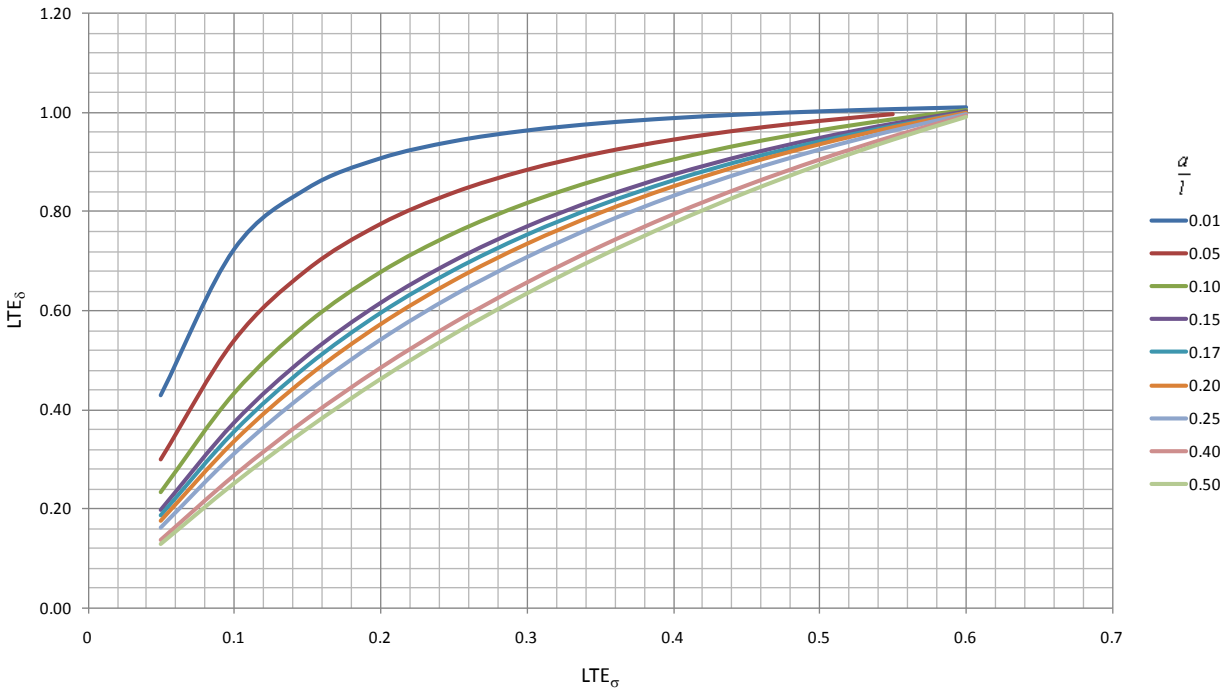

Figure 33. Relationship Between Stress-Based and Deflection-Based LTE for Different Values of Load Size Ratios (a/l)

Figure 34 shows the sensitivity of the PCC Modulus on stress-based and deflection based LTE curves. Figure 34 was generated considering the radius of the loaded area for (HWD) as 5.9 in, the thickness of the repair panel as 11 inches, and by varying the values of the concrete modulus from 1000 ksi to 5000 ksi.

The trends in Figure 34 clearly indicate that LTE_δ-LTE_σ curves are not sensitive to the values of PCC modulus. As previously shown in Figure 33, area of the load has the most impact on the sensitivity of the LTE_δ-LTE_σ curves.

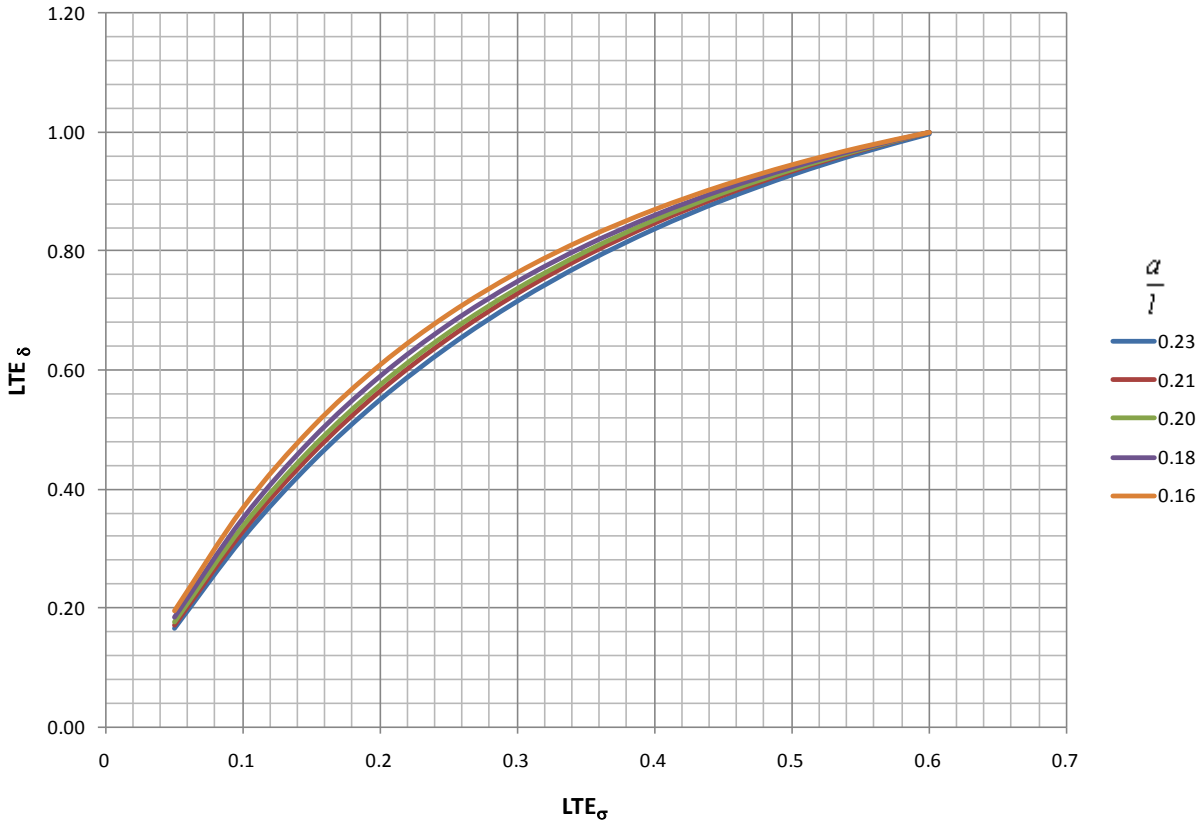

Figure 34. LTE_{δ}-LTE_{σ} Curves for Different Values of Concrete Modulus

The undamaged modulus values of the pre-existing concrete slabs were determined using iterative back calculation technique. The next section of this report presents the rationale behind using finite element analysis to back-calculate the layer stiffness properties. Figure 35 shows the design curve developed for calculation of the stress based LTE based on deflection based LTE.

The acceptance threshold for LTE_{δ} is designated as 0.7 (or 70%) and the cut off value is 0.3 (or 30%) for stress based LTE in the new Mechanistic Empirical Pavement Design Guide (MEPDG). The FAA also requires a minimum value of 0.25 when LT is used as design criteria [8].

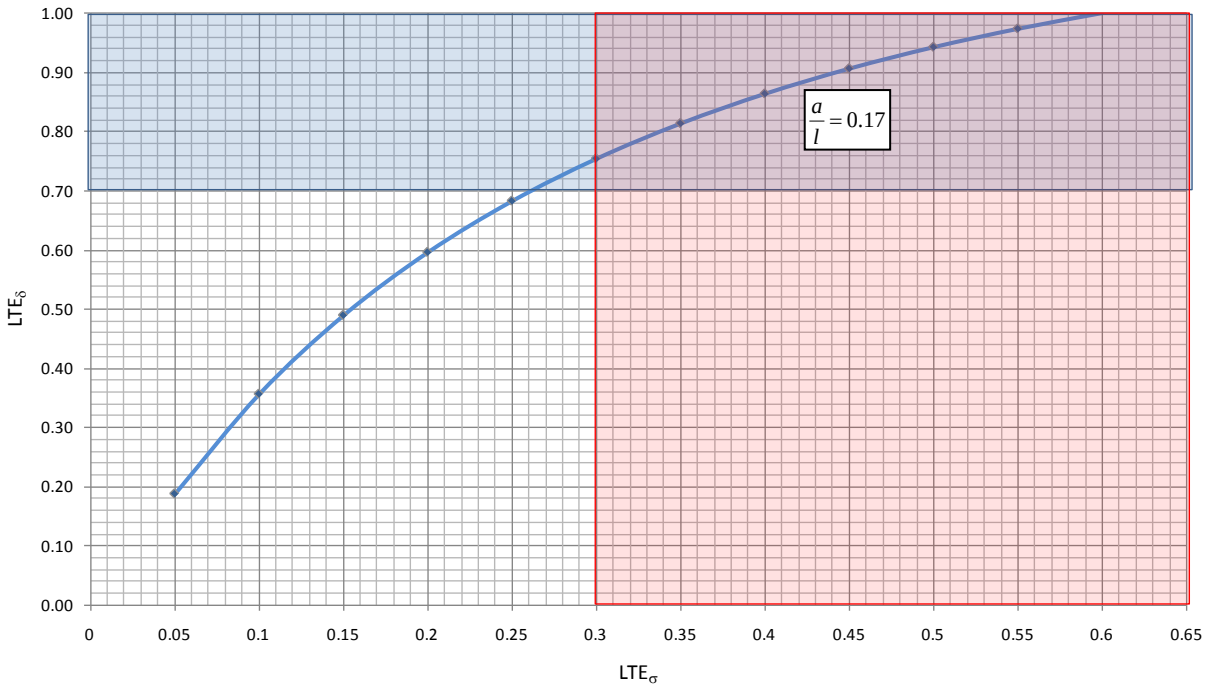

Figure 35. Graphical Representation of Acceptable Region in LTE_{δ} -LTE_{σ} Design Curve

5.1. Back Calculation of the Modulus of Pre-Existing Concrete Slabs

As previously discussed in this chapter, stiffness properties of the concrete slab significantly impact the distribution of aircraft loads between concrete panels. This section describes the mechanistic approach for back-calculation of the material properties and determination of the responses using finite element analysis. An HWD was used to determine the deflection basin. The measured deflections were in turn used to determine the material properties of each pavement layer.

In this part of the study the HWD load frame was placed at the middle of the pre-existing slabs for back-calculation of the modulus of pre-existing concrete slabs. This is due to the fact that mid-slab loading reduce/eliminate back-calculation errors imposed by discontinuity at the joints and boundary conditions in the finite element simulations. However, for the purpose of analysis of joint stiffness and LTE, the HWD load frame was placed at the edge of the slabs and the deflections were measured at two sides of the pre-existing slabs and repaired sections. Table 9 presents the deflections that resulted at the top of the pre-existing concrete panels due to HWD mid-slab loading.

Table 9. Deformations of Pre-existing Concrete Slabs Subjected to HWD Mid-slab Loading

Station	*Load (lbs)*	d_1	d_2	d_3	d_4	d_5	d_6	d_7
1	58,331	16.37	15.03	13.26	11.39	9.54	7.73	6.22
2	58,046	17.68	16.22	14.53	12.62	10.56	8.43	6.46
3	58,134	19.57	17.38	15.06	12.66	10.25	7.98	5.98
4	57,729	20.67	19.20	17.70	16.07	14.10	12.07	10.31
5	58,266	18.26	16.59	14.60	12.48	10.26	8.08	6.13
6	57,992	20.03	18.29	16.35	14.31	12.06	9.80	7.68
7	58,397	18.10	16.20	14.01	11.87	9.71	7.72	5.83
8	57,630	19.97	18.02	15.93	13.78	11.57	9.47	7.40
9	58,583	20.18	17.81	15.25	12.85	10.41	8.14	6.24
10	58,309	20.34	18.86	17.20	15.47	13.43	11.48	9.84
11	58,320	19.65	17.45	14.99	12.53	10.13	7.83	5.90
12	58,068	21.04	19.69	18.22	16.61	14.78	12.88	11.15
13	58,145	19.21	16.76	14.39	12.06	9.76	7.69	5.88
14	58,123	19.41	17.72	15.83	13.84	11.76	9.7	7.74
15	58,627	17.41	15.68	13.69	11.63	9.52	7.61	5.99
16	58,266	18.87	17.30	15.45	13.42	11.14	8.94	6.87
Mean		19.17	17.39	15.40	13.35	11.19	9.10	7.23
Standard Deviation		1.30	1.28	1.41	1.58	1.66	1.69	1.73
Coe. of Variation		6.76	7.36	9.18	11.80	14.82	18.62	23.90

The recorded plastic deformations were used to determine the deflection basin of the intact concrete slabs. Finite element (FE) approach was used to calculate the stresses and strains resulted from application of the HWD loading system. The measured surface deflections were in turn compared to the plastic deformations calculated using the finite element technique. Y-direction was considered as the direction of the travel. The load transfer devices (Dowel rods) were spaced 12 inches apart, perpendicular to the direction of the travel (Y-direction). LTE perpendicular to the direction of travel (X-direction) was considered as another variable in the simulations. Figure 36 shows plastic deformations on the surface of the concrete slab for one of the permutations of the experiment design.

Figure 36 illustrates the contour plot of deformations for the extreme scenario when the concrete modulus was considered as 1,000,000 psi and LTE_x as 90%.

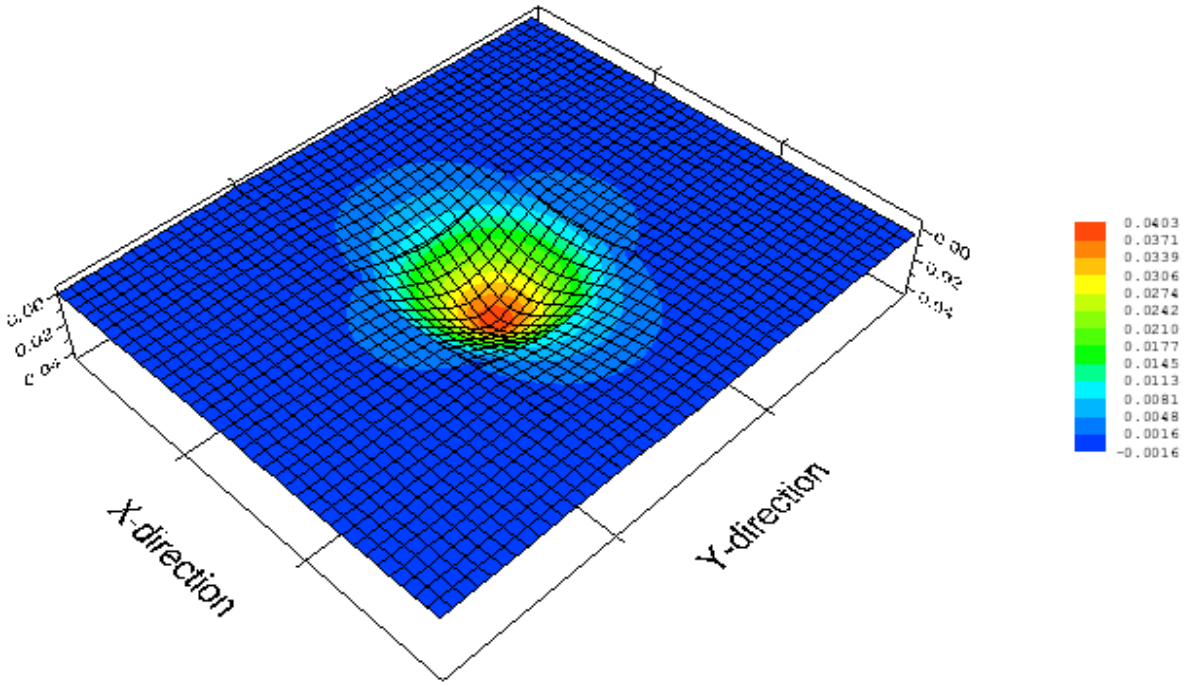

Figure 36. Contour Plot for Deflection Under HWD for LTEx=90% and Epcc=1000 ksi

Table 10 presents the ranges and the variables of the finite element simulations. The objective here is to iteratively find the material properties and LTE_x (across x-direction) that result in the best match between the measured deformations in the field and the calculated deformations using FE simulations.

Table 10. Variables of the Finite Element Simulations

Simulation ID	*LTE_x (%)*	*E_{pcc} (ksi)*	*FE Calculated ε_p*
1-90-1	90	1000	0.0407
2-90-1	90	2000	0.0336
3-90-1	90	3000	0.0381
4-90-1	90	4000	0.0259
5-90-1	90	5000	0.0249
1-95-2	95	1000	0.0403
2-95-2	95	2000	0.0378
3-95-2	95	3000	0.0333
4-95-2	95	4000	0.0256
5-95-2	95	5000	0.0246
1-100-3	100	1000	0.0349
2-100-3	100	2000	0.0320
3-100-3	100	3000	0.0270
4-100-3	100	4000	0.0184
5-100-3	100	5000	0.0172

Figure 37 and Figure 38 shows the significance of LTE in X-direction and its impact on the calculated responses using finite element approach. Figure 37 shows the contour plot of the plastic deformations at the surface of the concrete when LTE_x is considered to be 100 percent. Figure 38 shows the same simulation but when the LTE in X-direction is reduced to 90 percent. Figure 37 and Figure 38 suggest that maximum deflection under the HWD load at the center of the slab has increased about 26 percent when LTE in X-direction was reduced from 100 to 90 percent. This clearly indicates the significance of the LTE perpendicular to the direction of travel on the distribution of the loads. Therefore, in the experiment design presented in Table 10, LTE in X-direction was also considered as a variable.

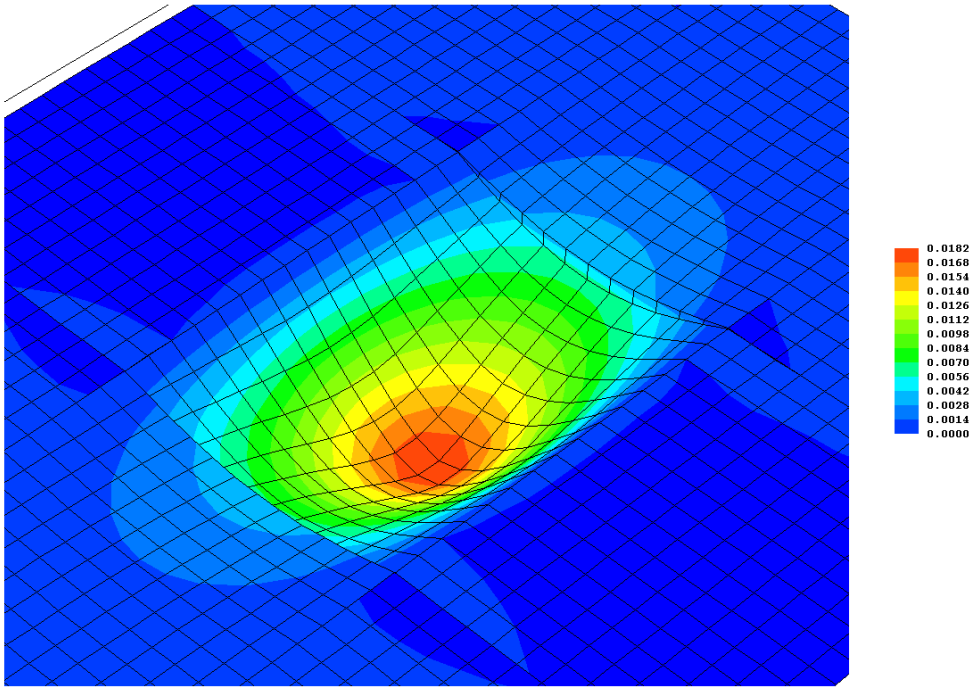

Figure 37. Contour Plot of the Deflections for Mid-slab Loading for Epcc=4000 ksi and LTEx=100%

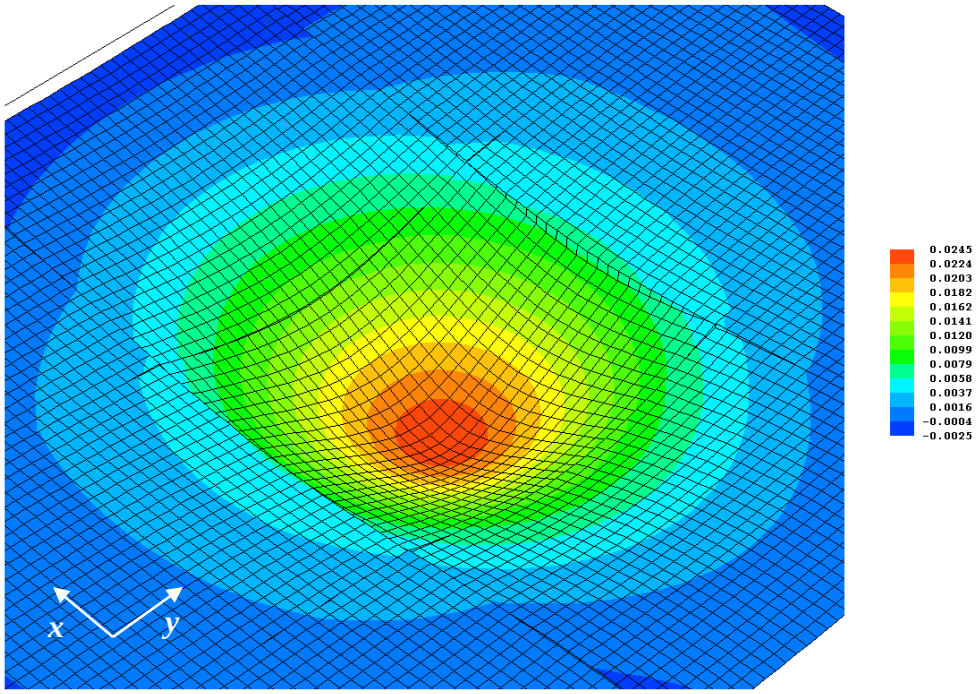

Figure 38. Contour Plot of the Deflections for Mid-slab Loading for Epcc=4000 ksi and LTEx=90%

Figure 39, Figure 40, and Figure 41 show the distribution of the stresses and deformations that resulted from finite element analysis of the rigid pavement system. Figure 39 shows the distribution of the vertical stresses at the top of the subgrade when LTE_x=90 percent and the concrete modulus was assumed to be 5,000,000 psi. This plot shows that maximum vertical stress happens at the centerline of the HWD loading system and the stresses reduce in nonlinear fashion with offset from the load plate.

Figure 38 indicates that stresses calculated in the adjacent slabs are not zero. Therefore, this plot shows the contribution of the adjacent slabs and the supporting foundation to distribute the stresses imposed by the HWD loading system. This plot also shows different stress distribution patterns in the direction of travel (Y-direction) and the direction perpendicular to the direction of aircraft operations (X-direction). This is due to the fact that load transfer devices (dowel rods) were located in the direction of travel and the load transfer in X-direction was assumed as a constant number along the joint in X-direction.

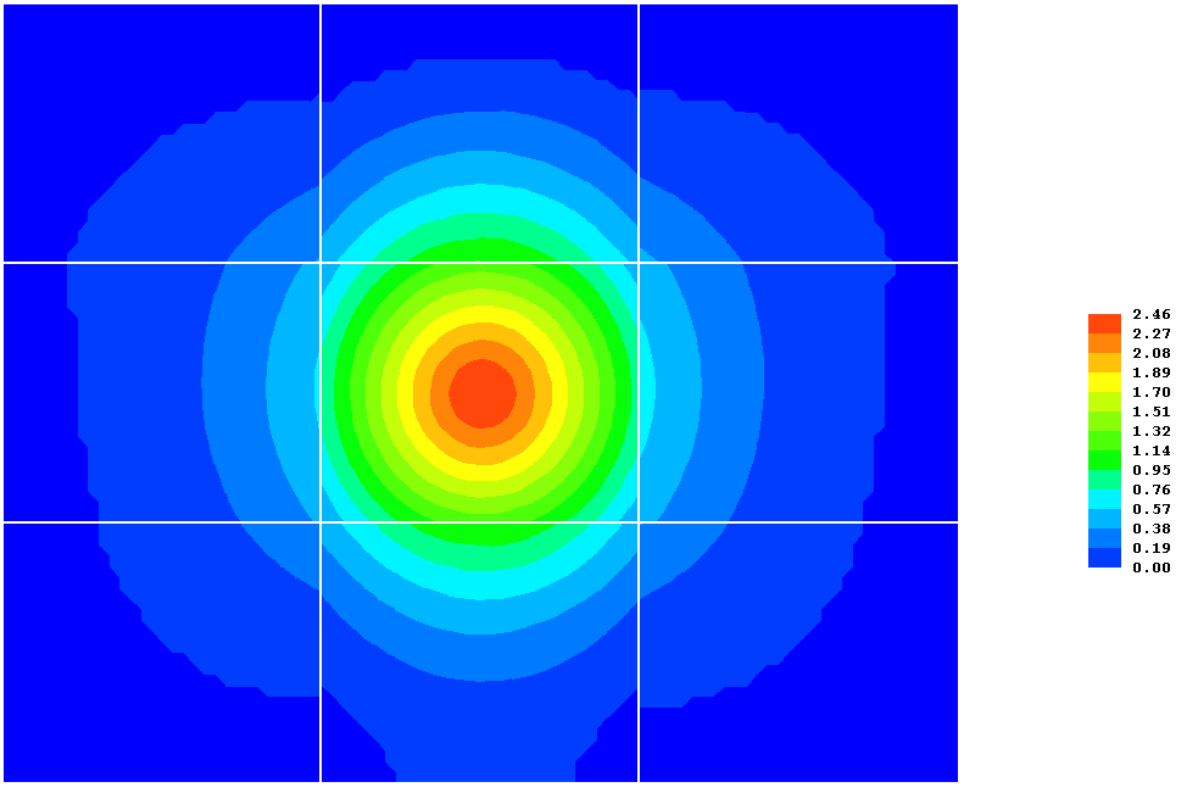

Figure 39. Distribution of Vertical Stresses at the Top of the Subgrade for LTEx=90% and E_{Pcc}=5000 ksi

Figure 40 and Figure 41 shows the distribution of shear stresses at the top of concrete slabs and distribution of vertical stresses at the top of base layer, respectively. Figure 40 shows the shear stress reversal under the load. As expected, shear stress is zero under the load centerline and is compressive in nature at one side of the load and tensile on the other end. The sign of the shear stress depends on the direction of the moving load.

Figure 41 illustrates the distribution of vertical stresses at the top of the base layer. This plot clearly indicates difference between the pressure bulbs in the direction of travel (Y-direction) and the direction perpendicular to aircraft load (X-direction). As previously discussed, this is due to different assumptions for load transfer at the two sides of the slabs.

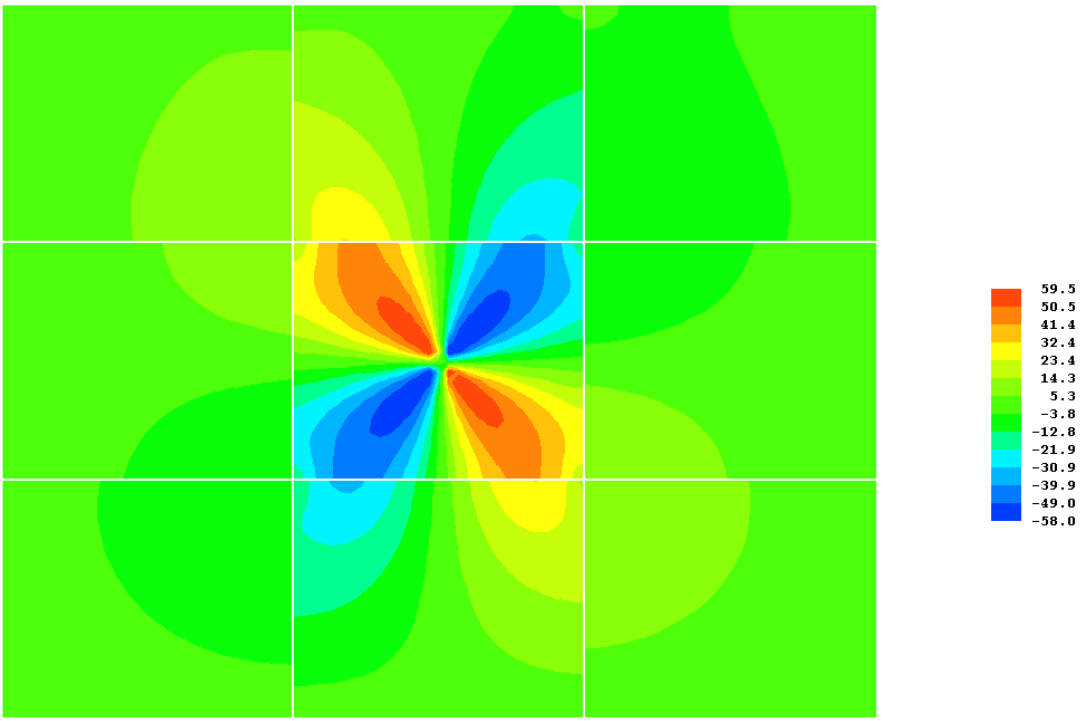

Figure 40. Distribution of Shear Stresses at the Top of the PCC for LTEx=90% and Epcc=5000 ksi

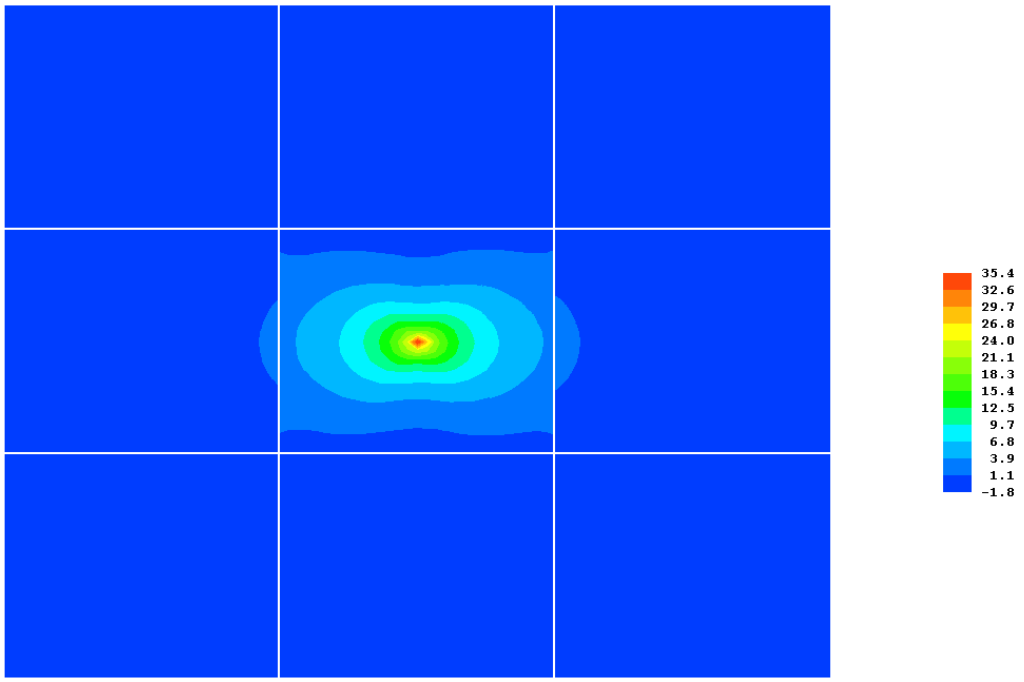

Figure 41. Distribution of Vertical Stresses at the Top of the Base Layer for LTEx=90% and Epcc=5000 ksi

5.2. Analysis of Load Transfer Efficiency for Precast Panels

This section presents the analysis results for the load transfer efficiencies based on different criteria. An HWD was used to induce non-recoverable plastic deformations at the joint and the deflections were measured at several radial distances from the impact load. The sections were trafficked using an F-15 load cart to study the deterioration of joint stiffness with number of load applications. Load transfer was in turn determined at each loading interval to capture the effect of load repetition on the loss of load transfer for different permutations of the experiment design.

5.2.1. Deflection-Based Load Transfer Efficiency (LTE_δ)

Figure 42 presents the trends of LTE_δ based on direct measurements of plastic deformations using HWD. Equation 1 was used to calculate the LTE_δ for each permutation and at each loading interval.

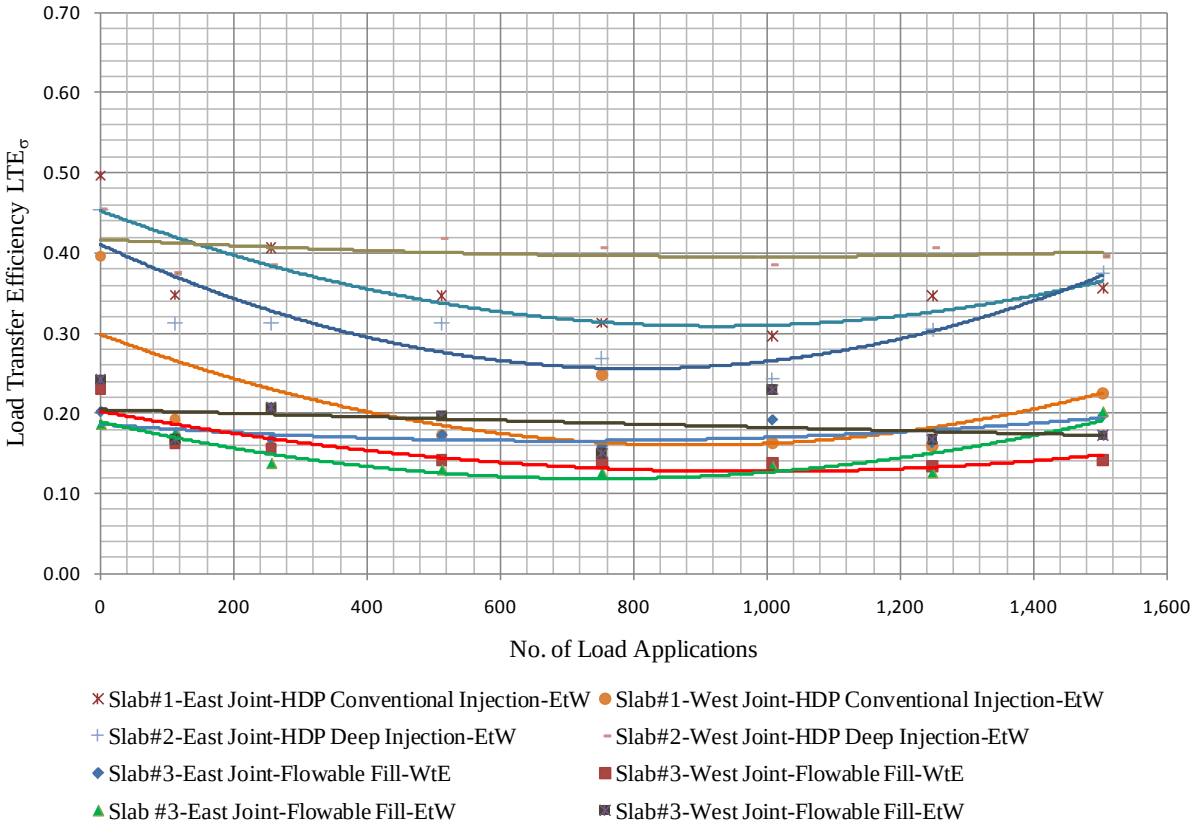

Figure 42. Deflection Based Load Transfer Efficiency (LTE_δ) for Variants of the Experiment Design

The measurements were taken at two sides of the joints. In other words the at each load interval, the HWD was placed at each side of the joints and directional load transfer efficiencies were determined.

As illustrated in Figure 42, load transfer at the west joint of Slab #2, which was installed with deep injection method, had the highest value of LTE throughout the testing period. The calculated values of the deflection based LTE satisfy the requirement set by MEPDG [13].

Slab #1, with high density polyurethane as bonding agent, did not have as high of a LTE compared to Slab #2. Slab #3, with flowable fill, was found to perform worst compared to the other design variants. LTE plots presented in Figures 42 to 44 can be used an indication of the relative performance for different variants of the experiment design.

Another set of deflection-based load transfer LTE_{δ}^{*}, were calculated using Equation 4. The trends and performance raking based on LTE_{δ}^{*} were essentially the same for the factorial design. The results of this set of LTE_{δ}^{*} calculations were tabulated in Appendix B of this report.

5.2.2. Stress-Based Load Transfer Efficiency (LTE_{σ}).

Figure 43 shows the results for stress based LTE calculated using Equation 10. The results indicate that Slab #2 outperformed Slab #1 and Slab #3 in terms of higher LTE_{σ} values. Similar to the deflection-based LTE, Slab #2 had consistently high values of LTE_{σ} at various loading intervals.

Slab #3, with flowable fill, had the lowest LTE compared to its counterparts. Repaired sections with higher values of LTE are expected to perform better in terms of orthogonal load bearing capacity.

Note that there is no one to one relationship between LTE_{δ} and LTE_{σ} and the criterion are nonlinearly related as indicated in Equation 10. As indicted earlier in this chapter, stress based LTE and deflection based LTE have different ranges. LTE_{σ} ranges from zero for the worst load transfer performance to 0.6 for ideal load transfer capacity, while LTE_{δ} ranges from zero to one. Results from Figure 42 and Figure 43 clearly suggest superiority of performance for the slabs with high density polyurethane as bonding agent, compared to flowable fill.

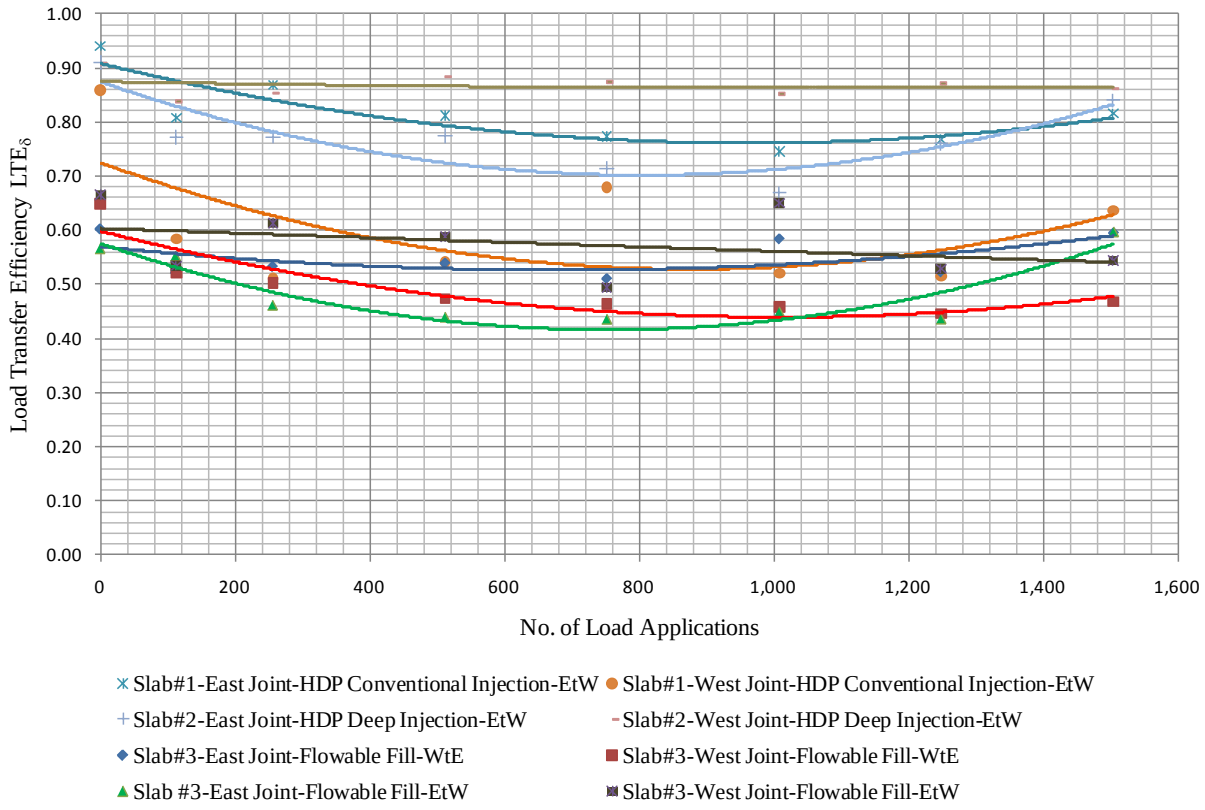

Figure 43. Stress Based Load Transfer Efficiency (LTE_σ) for Variants of the Experiment Design

5.2.3. FAA Criteria (LT)

The FAA parameter for measuring LT derives from stress-based LTE calculations. The relationship between stress based LTE and LT is presented in Equation 6. According to the FAA design guide, the acceptable minimum value for LT is 0.25. The design should be revised if the load transfer does not meet this requirement.

Figure 44 shows the LT values calculated using Equation 6 for the experiment design permutations. The results indicate that Slab #2 performs better in terms of LT compared to the other counterparts. Slab #1 did not perform as well as Slab #2 and Slab #3 with flowable fill performs significantly lower compared to slabs with HDP foam. The result confirms the observations and analysis results presented in Figures 41 and 42 using LTE_σ and LTE_δ as LTE criteria. Comparisons of load transfer efficiencies at two sides of the joints are presented in Appendix B and Appendix C.

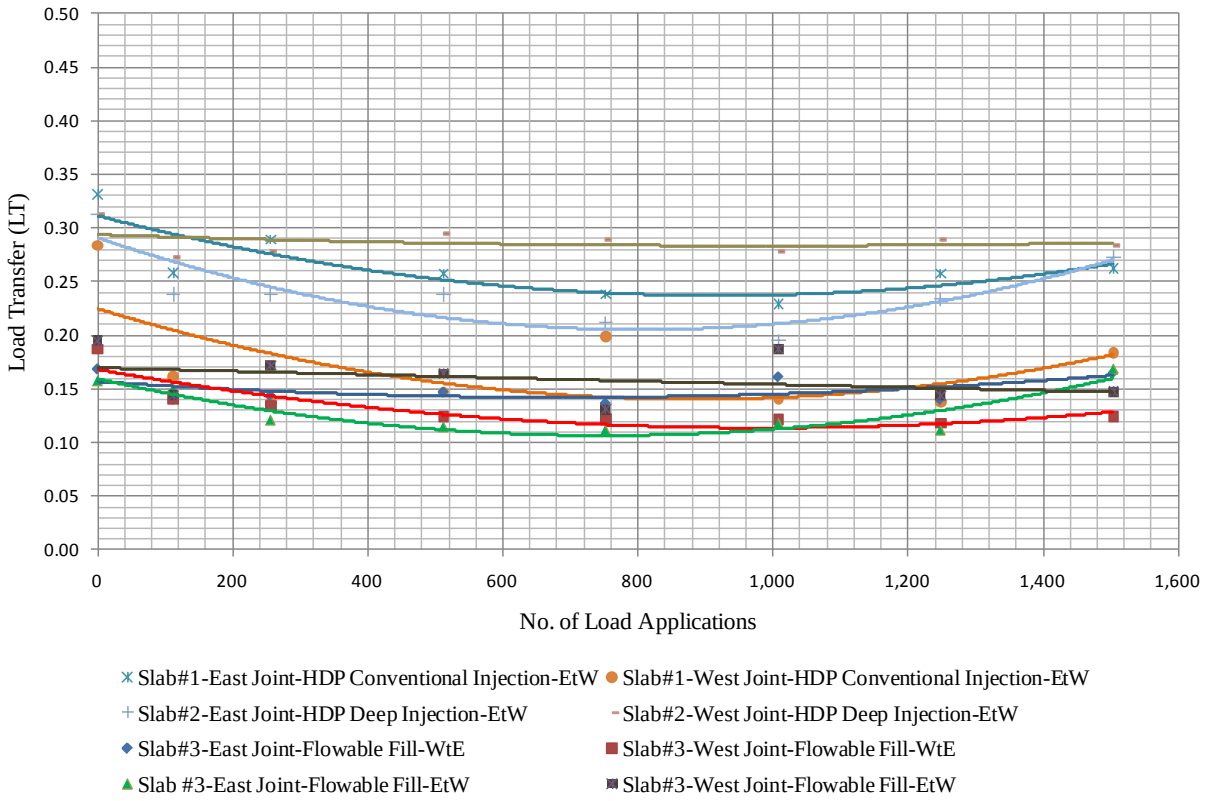

Figure 44. FAA Criteria forLoad Transfer Efficiency (LT) for Variants of the Experiment Design

5.3. Analysis of Performance Based on Joint Stiffness

Stability of joints and its resistance to orthogonal movement is an important factor that influences the load transfer capability of the repaired sections. There are three load transfer mechanisms perceived for precast repair sections:

- Load transfer through aggregate interlock
- Load transfer through reinforcement (dowel rods)
- Load transfer through foundation support

5.3.1. Load Transfer through Aggregate Interlock (LTE_{AGG})

According to the mechanistic empirical pavement design guide (MEPDG), load transfer through aggregate interlock is a function of joint stiffness which in turn is related to shear capacity of the joints [13]. Load transfer through frictional forces between the aggregate particles can be determined by Equation 11.

$$LTE_{AGG} = \frac{100}{1+0.012\, J_{AGG}^{-0.849}} \quad (11)$$

Where:

LTE_{AGG}= Load transfer through aggregate interlock

J_{AGG}= transverse joint stiffness

Transverse joint stiffness in Equation 12 can be found as a function of shear capacity of the aggregate particles which is influenced by aggregate geometry (angularity, form, and texture of particles) as well as particle size distribution in the mix. Particle angularity refers to broken edges at the corner of aggregates, *form* corresponds to sphericity of the particles and texture refers to small asperities at the surface of the particles. Micro-texture of the particle plays an important role in aggregate interlock. Therefore, mixes consisting of less polished aggregates are expected to perform better in terms of higher shear capacity compared to mixes with smooth aggregates. The MEPDG suggests the following relationship exists between joint stiffness and shear capacity of the joint [13]:

$$Log\ (J_{AGG}) = -28.4\ e^{-0.35-\left[\frac{S-0.35}{0.38}\right]} \quad (12)$$

Where:

J_{AGG}=transverse joint stiffness
S=shear capacity of the joint at the first loading interval

Shear capacity of the joint is influenced by joint spacing and thickness of the concrete slab. Initial shear stiffness of the joint can be determined by Equation 13:

$$S = 0.05\ h_{pcc}\ e^{0.032\ jw} \quad (13)$$

Where:

h_{pcc}= thickness of the concrete
jw= joint spacing

Equations 11 through 13 were used to determine the load transfer through aggregate interlock (LTE_{AGG}).

5.3.2. Load Transfer through Reinforcement (LTE_{DOWEL}).

Load transfer and stiffness of the joints in reinforced concrete slabs can be determined using Equation 14:

$$LTE_{DOWEL} = \frac{100}{1+0.012\ J_d^{-0.849}} \quad (14)$$

Where:

LTE_{DOWEL}= load transfer due to presence of reinforcement such as dowel rods
J_d= non-dimensional dowel rod stiffness which can be found from Equations 15 and 16:

$$J_d = J_d^* + (J_0 - J_d^*)\exp(-d) \quad (15)$$

$$J_0 = \frac{120\ d^2}{h_{PCC}} \quad (16)$$

Where:

J_0=initial dowel rod stiffness
J_d^*= critical dowel rod stiffness
d=dowel rod diameter, in
h_{pcc}=thickness of the concrete slab, in

Critical dowel rod stiffness can be found from Equation 17:

$$J_d^* = Min\left\{118, Max\left[165\frac{d^2}{h_{pcc}} - 19.8120, 0.4\right]\right\} \quad (17)$$

5.3.3. Load Transfer through Foundation Support (LTE $_{Foundation}$)

The mechanistic MEPDG suggests using the values presented in Table 11 to determine the (***LTE*** $_{Foundation}$) component of load transfer [13].

Table 11. Foundation Load Transfer for Different Base Types

Foundation Type	***LTE*** $_{Foundation}$
Unbound Aggregate Base	20%
Cement Treated or Asphalt Treated Base	30%
Lime Treated Base	40%

As described earlier in section 5.3, the total load transfer efficiency LTE $_{Total}$ can be decomposed into three components: 1) load transfer due to joint stiffness and aggregate interlock LTE $_{AGG}$, 2) load transfer through reinforcement LTE $_{Dowels}$ and 3) load transfer through foundation support LTE $_{Foundation}$. The relationship between the components of LTE $_{Total}$ and the material properties is described in Equation 18 [14]:

$$LTE_{Total} = 100\left\{1 - \left[1 - \frac{1}{1+log^{-1}\left[\frac{(0.214-0.183\left(\frac{a}{l}\right)-[\log(J)+R])}{1.18}\right]}\right]\left[1 - \frac{LTE_{Foundation}}{100}\right]\right\} \quad (18)$$

Where:

a=radius of the load in HWD, in
l=radius of relative stiffness
J=Load transfer provided by aggregate interlock
R=load transfer provided by steel reinforcement
LTE_{Total}=total load transfer efficiency provided by aggregate interlock, steel reinforcement and foundation support.

Figure 45 shows the joint stiffness values of the design variants after 1,504 applications of the F-15 load cart. The joint stiffness was assumed to be a function of aggregate interlock and load transfer devices, such as dowel rods in the precast panels. The results indicate concrete panels installed by heavy density foam as bonding agent performed better in terms of higher joint stiffness, compared to variants installed with flowable fill. On the other hand, Slab #2 was found to have higher joint stiffness compared to Slabs #1 and #3. This suggests that Slab #2, installed using deep injection method, performed better compared to the other permutations of the design experiment.

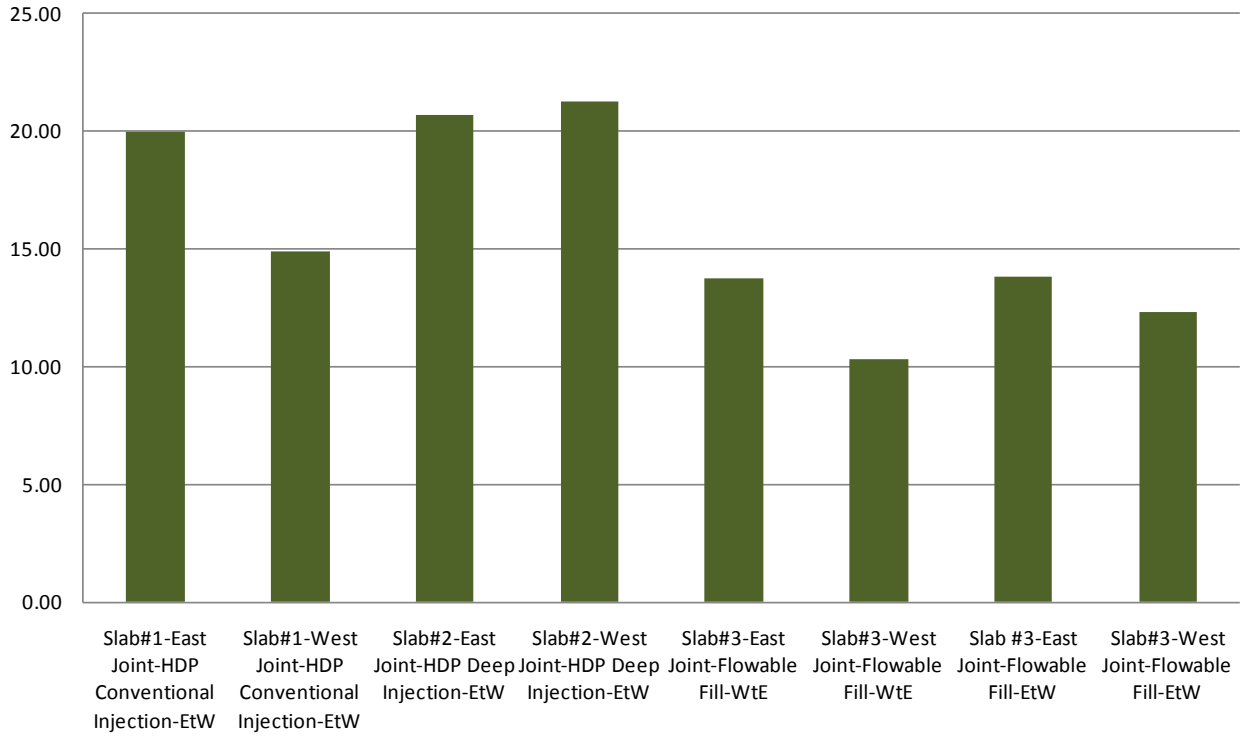

Figure 45. Joint Stiffness after 1504 Applications of F-15 Load Cart

Figure 46 shows initial joint stiffness and joint stiffness after 1,504 load applications. This plot again confirms that slabs installed with high density polyurethane have better initial and terminal joint stiffness than Slab #3, which was installed using flowable fill as a leveling mechanism.

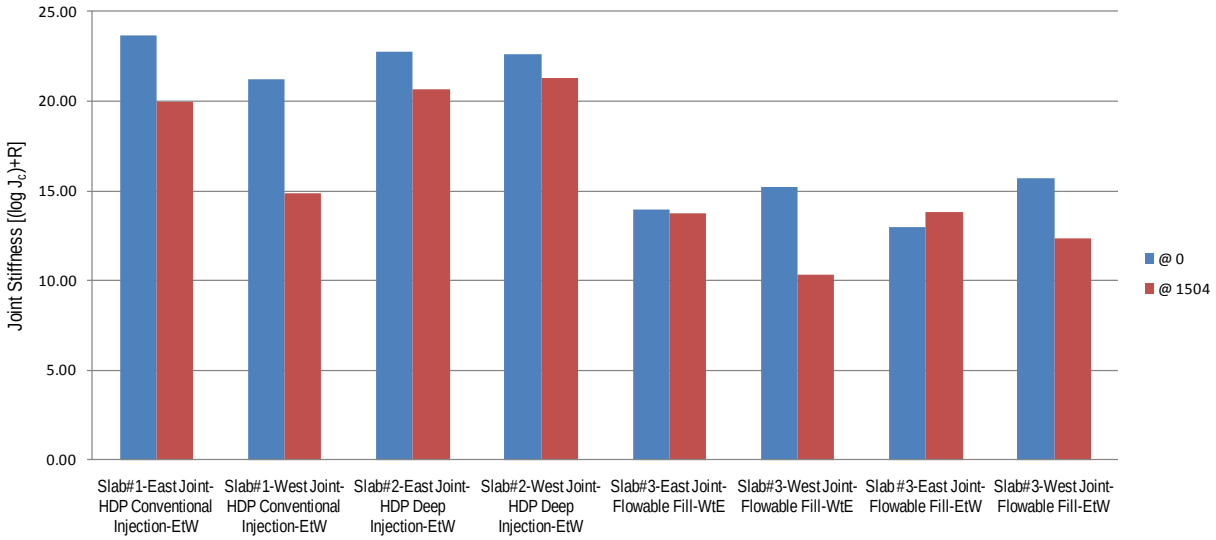

Figure 46. Comparison Between Initial and Terminal Joint Stiffness

Figure 47 shows the percentage loss of joint stiffness due to 1,504 load applications. This plot suggests that deep injection method resulted in better systems in terms of smaller loss of joint stiffness. In other words, the gradient of the loss of stiffness in precast panels with HDP foam and installed with deep injection method is relatively smaller than the other methods. The results pertaining to joint stiffness were in conformity with the LTE and LT results presented in previous section.

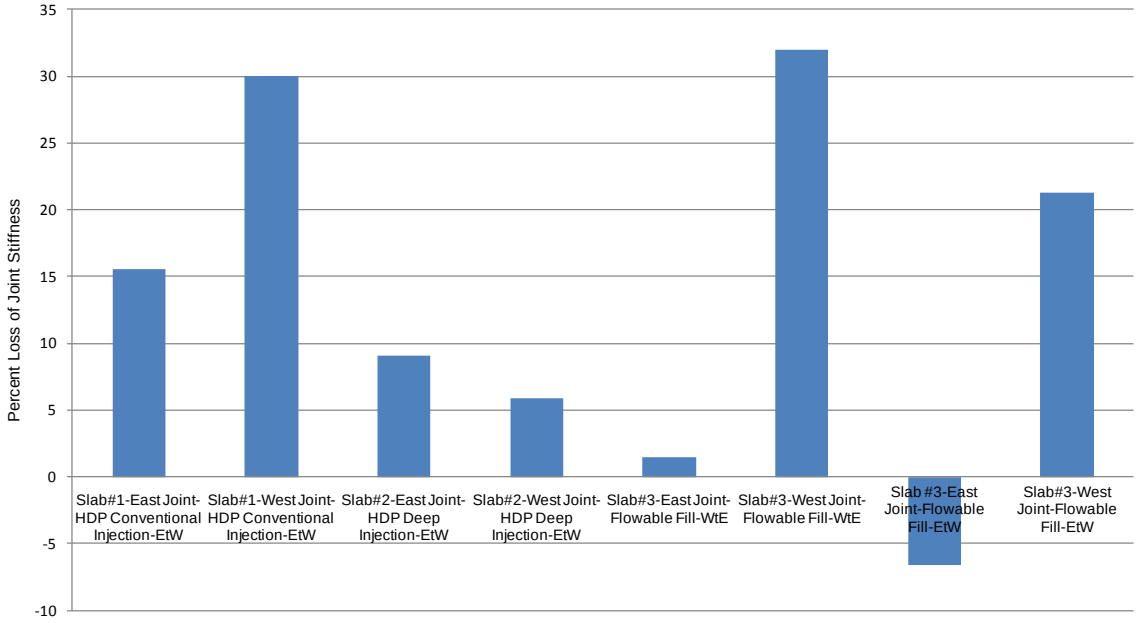

Figure 47. Loss of Joint Stiffness After 1504 Applications of F-15 Load Cart

5.4. Deformation Energy Concept

One of the damage mechanisms considered in the analysis of the precast panels is assumed to be due to the loss of support and deformation of the supping slab foundation. Deformation energy concept was employed to characterize the amount of energy dissipated through the subgrade soil using different installation techniques. The plastic deformation induced by aircraft loads under the subgrade results in faulting or differential elevation between the precast panels and pre-existing concrete slabs. The dissipated energy concept was originally developed by Larralde to characterize pumping and faulting potential in rigid pavements [15, 16].

In the differential energy concept, the dissipated energy is assumed to be proportional to the elastic deformation energy inflicted to the subgrade. The density of the elastic deformation can be written as Equation 19 [17]:

$$E = \frac{1}{2}\, q\, \epsilon_p \tag{19}$$

Where:

E= density of elastic deformation
q= pressure at slab-subgrade interface
ϵ_p= plastic deformation of the top of the subgrade

Assuming the slab foundation follows Winkler subgrade model, the stiffness of the subgrade and the interface pressure are related as shown in Equation 20:

$$q = k\,\epsilon_p \tag{20}$$

Where *k* is the modulus of subgrade reaction and characterizes the stiffness properties of the foundation. By substituting Equation 20 into Equation 19 we have Equation 21:

$$E = \frac{1}{2}\,k\,\epsilon_p^2 \tag{21}$$

Differential energy (DE) between the repaired section and pre-existing slabs can be determined with Equation 22:

$$DE = E_u - E_l = \left[\frac{1}{2}\,k\,\epsilon_p^2\right]_u - \left[\frac{1}{2}\,k\,\epsilon_p^2\right]_l = \frac{1}{2}\,k\,\left[\epsilon_{p_u}^2 - \epsilon_{p_l}^2\right] \tag{22}$$

Equation 22 can also be written as Equation 23:

$$DE = \frac{1}{2}\,k\,\left(\epsilon_{p_u} - \epsilon_{p_l}\right)\left(\epsilon_{p_u} + \epsilon_{p_l}\right) \tag{23}$$

Where:

DE= differential energy
$(\epsilon\varepsilon_p)_R$= plastic deformation on the top of the subgrade for the unloaded slab
$(\epsilon_p)_P$= plastic deformation on the top of the subgrade for the loaded slab
k= modulus of the subgrade reaction

The term $\left(\epsilon_{p_u} + \epsilon_{p_l}\right)$ is referred to as free cumulative deflection and represents the flexibility of the slab-joints system. Slab-joint systems with higher free cumulative energy represent systems with higher deformation energy and therefore are more prone to deterioration due to faulting.

On the other hand, the term $\left(\epsilon_{p_u} - \epsilon_{p_l}\right)$ is referred to as differential settlement between the repaired section and pre-existing slab. This term characterizes the relative movement between the two slabs. Slab-joint systems with greater relative settlement are more prone to loss of joint stiffness and damage due to faulting. The differential settlement depends on the efficiency and mechanism of load transfer between the repaired section and pre-existing concrete slab as well as stiffness of the supporting foundation. As previously discussed in this chapter, LTE can be calculated based on the deflections of repaired panel and pre-existing slab with Equation 24:

$$LTE = \frac{(\epsilon_p)_u}{(\epsilon_p)_l} \times 100 \tag{24}$$

The relationship between LTE and deformation energy, shown in Equation 25, can be derived using Equations 6 and 7.

$$DE = \frac{1}{2}\,k\,\left(\epsilon_{p_u} + \epsilon_{p_l}\right)\left(\frac{1-LTE}{1+LTE}\right) \tag{25}$$

Equation 25 shows the impact of LTE on the energy dissipated from the concrete slab to the subgrade. This energy transfer resulted in non-recoverable strains at the top the subgrade. Therefore, in this study, DE concept was employed to determine which combination of leveling/lifting techniques will result in less dissipated deformation energy of the runway foundation.

5.4.1. Analysis of Performance Based on Deformation Energy

Figure 48 presents the deformation energy results for eight variants of the design experiment. Dissipated deferential energy was calculated based on the HWD deformations on the loaded and unloaded slabs. A radar type chart was selected to plot the variation of deformation energy after each load interval. This graphical method of displaying the analysis results provides intuitive and insightful understanding of the interactions between multivariate data.

Radar charts, also referred to as star charts, consist of a sequence of equi-angular spokes called radii. Each spoke in Figure 48 refers to a specific loading interval. In this study, deflections were measured using HWD after 0, 112, 256, 512, 752, 1008, 1248 and 1504 applications of the F-15 load cart. The value of the calculated deformation energy at each interval was plotted on the corresponding spoke. The connected dots create a polygon for each permutation of the experiment design. Polygons with smaller area correspond to permutations with smaller deformation energy while larger polygons refer to less favorable variants with higher deformation energy. Polygons with smaller surface area are believed to perform better in the field. This plot also indicates which variants performed similarly in terms of dissipated deformation energy. Variants with close polygon area are expected to perform similarly in the field.

Figure 48 shows Slab #2 at west joint, which was installed with deep injection method, has the smallest polygon area and therefore performed better in terms of dissipated deformation energy. After the polygon referring to Slab #2 at west joint, areas of the polygons corresponding to Slab #1 have smaller areas compared to other permutations of the experiment design as illustrated in Figure 47. This suggests that Slab #1, at east and west joints, performed superior in terms of lower deformation energy. Slab #3 was found to have the highest area compared to other variants and therefore ranked last in terms of performance based on deformation energy.

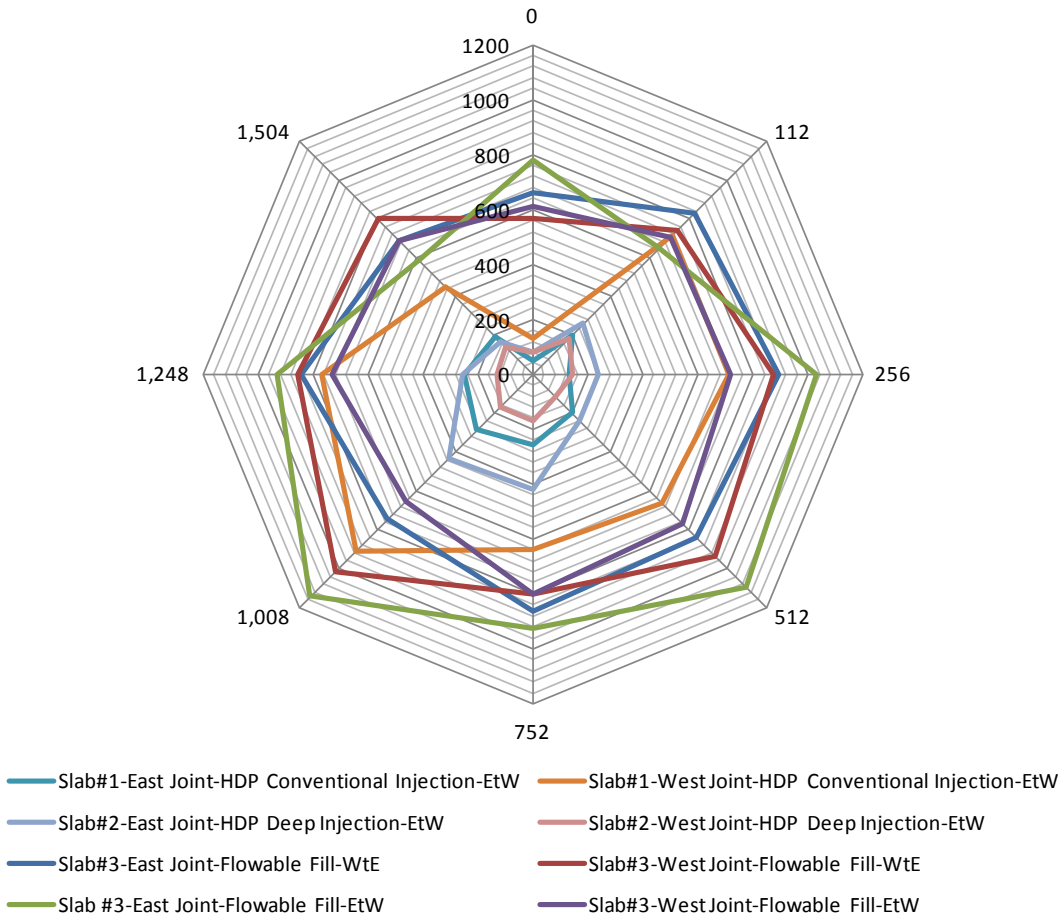

Figure 48. Analysis of Performance Based on Deformation Energy

6. CONCLUSIONS

Three precast concrete repair panels, each utilizing an alternative base preparation method, were installed and subjected to accelerated traffic loading with an F-15 load cart. The three methods included:

1) Conventional HDP injection (HDP injection directly underneath the precast concrete repair panel),
2) Deep HDP injection (HDP injection 36 inches underneath the precast concrete repair panel), and
3) Flowable fill (placed immediately prior to precast concrete panel placement).

Deformations imposed by application of HWD for each slab were collected before, during, and after the loading process to assess the effectiveness of each base preparation method. Additionally, installation procedures and timelines were recorded.

Installation included removal of the distressed slab and placement of the precast concrete repair panel into the repair area. Two concrete cutting saws, a wall-saw and a walk-behind concrete saw, were utilized to remove the distressed PCC section from the surrounding PCC slab. The walk-behind saw significantly out-performed the wall-saw and substantially reduced the time required to cut the distressed area from the adjacent PCC slab. An appropriately rated crane was used to remove the distressed slab and subsequently position the precast concrete repair slab into the repair area. Load transfer performance of the three precast concrete repair panels is summarized in the following paragraph.

Performance of the repaired sections was characterized by LTE, joint stiffness and deformation energy dissipated through the pavement foundation. HWD testing, along with a F-15 gear simulator, were used to determine the stiffness properties and accumulation of plastic deformations after each load interval. Deterioration of joint stiffness and LTE, as well as increase in deformation energy, were calculated as a function of the number of load applications. The results indicate significant increase in the deformation energy and considerable loss of joint stiffness with number of load applications when flowable fill was used as leveling material. This study reveals that precast panels installed with high density polyurethane foam performed superior compared to precast panels installed with flowable fill. Additionally, precast panels installed using deep injection method performed better in terms of higher LTE, higher joint stiffness and lower dissipated deformation energy. Figure 49 summarizes the performance ranking order of the sections tested in this study. This study suggests that precast concrete panels bonded with high density polyurethane foam and installed using deep injection method performed best compared to other design permutations.

Installation times, beginning with demarcation of the distressed slab and ending with joint sealing of the precast concrete panel, were as follows: 1) Flowable fill (255 minutes), 2) HDP conventional injection (335 minutes), and 3) HDP deep injection (380 minutes).

Flowable fill, despite the abbreviated timeline, was significantly outperformed and is a sub-optimal option when compared to the two HDP injection methods. Additionally, HDP installation times, conventional and deep injection, are expected to decrease significantly with

repetition. It is likely that the disparity between the two HDP injection methods will also decrease, and the deep injection timeline will approach the conventional installation timeline.

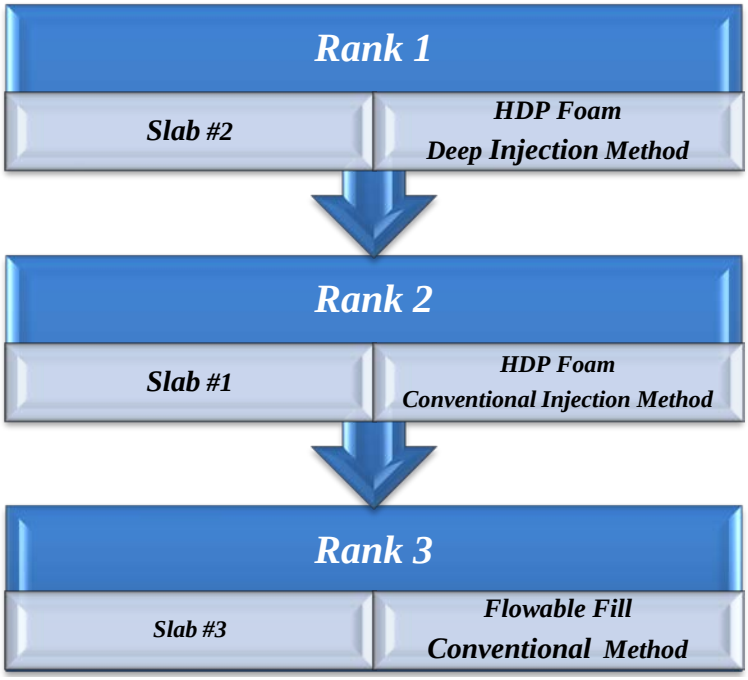

Figure 49. Performance Order of the Tested Sections

7. RECOMMENDATIONS

Performance of the concrete pavements is greatly impacted by environmental effects such as temperature and humidity. Proper characterization of the responses under the load should account for curling and warping stresses induced by temperature variations and climatic cycles. Since the focus of this study was to compare different installation (leveling/lifting) techniques, test sections were assumed to experience similar climatic conditions and the effect of temperature variation was not factored in the FE analysis of the repaired sections. However, for mechanistic response analysis and thickness design of the repaired panels, it is imperative to account for thermal stresses induced by temperature variation.

Layered elastic solutions were used to model and calculate the responses of the unbound granular base layer subgrade subjected to the F-15 load cart and HWD loading system. Layered elastic modeling of the pavement foundations results in unrealistic tensile stresses at the bottom of the base layer and subgrade. Recent advances in modeling the particular systems indicate that anisotropic modeling of granular materials eliminate this discrepancy and provides more realistic stresses and strains under the load [18]. Therefore the anisotropic solution should be used for proper characterization of the granular layers.

AFRL recommends the following:

1) Use the HDP deep injection method to maximize LTE between precast concrete repair panels and the surrounding PCC slab.

2) Utilize a walk-behind concrete saw to remove the distressed portion of the slab from the surrounding PCC slab.

3) Construct an adjustable rigid mold to fabricate precast panels of variable dimensions.

4) Integrate load transfer dowel rods into the precast panel and constructing dowel slot receptacles in the existing concrete.

5) Perform accelerated loading test accompanied by non destructive testing of the panels at two different times of the year, preferably one hot summer day and one cold winter day, to characterize the impact of environmental effects such as temperature and relative humidity on the load transfer efficiency of the precast panels.

8. REFERENCES

1. Voigt, G.F., "Fast Full-Depth Pavement Repair," Report RP334P, American Concrete Pavement Association.

2. Olidis, Chris, Swan, D.J., Saeed, Athar, et al., "Repair of Airfield Rigid Pavements Using Concrete Panels," Technical Report AFRL.RX.TY.2009-4588, Tyndall Air Force Base, Air Force Research Lab Materials and Manufacturing Directorate, 2009.

3. An Overview of the Super-Slab® System. Fort Miller Co. [Online] [Cited February 2, 2010.] www.super-slab.com

4. Hossain, S., Ozyildirim, C., and Tate, T.R., "Evaluation of Precast Patches on U.S. 60 Near the New Kent and James City County Line," Report VTRC 06-R22, Virginia Transportation Research Council, 2006.

5. Pavement Lifting. UretekUSA Co. [Online] [Cited February 16,2010] www.uretekusa.com

6. Swift Lift® System. Dayton Superior. [Online] [Cited March 5, 2010] www.daytonsuperior.com

7. Hammons, M.I. and Ioannides, A.M., "Advanced Pavement Design: Finite Element Modeling for Rigid Pavement Joints. Report I: Background Investigation", DOT/FAA/AR-95/85, 1997.

8. Tabatabie, A.M. and Barenberg, E.J., "Structural Analysis of Concrete Pavement Systems,"*ASCE, Transportation Engineering Journal.* Vol. 106, No. 5, 1980, pp. 493-506.

9. Khazanovich, L. and Gotlif, A., "Evaluation of Joint and Crack Load Transfer – Final Report", FHWA-RD-02-088, 2003.

10. Hammons, M.I. , "Advanced Pavement Design: Finite Element Modeling for Rigid Pavement Joints. Report II: Model Development", DOT/FAA/AR-97/7, 1998.

11. Ioannides, A.M. and Hammons, M.I., "A Westergaard-Type Solution for the Edge Load Transfer Problem", Transportation Research Board, *Transportation Research Record No. 1525*, Washington, D.C., 1996, pp. 28-34.

12. Ioannides, A.M., and Korovesis, G.T., "Analysis and Design of Doweled Slab-On-Grade Pavement Systems." ASCE, *Journal of Transportation Engineering*, Vol. 118, No. 6, New York, 1992, pp. 745-768.

13. ARA, Inc. "Guide for Mechanistic- Empirical Design of New and Rehabilitated Pavement Structures- Appendix JJ: Transverse Joint Faulting Model," NCHRP Project 1-37A Report, Transportation Research Board, National Research Council, Washington, D.C. 2004.

14. Crovetti, J.A. and Darter M.I., “Void Detection for Jointed Concrete Pavements” *Transportation Research Record 1041*, Transportation Research Board, National Research Council, Washington, D.C., 1985, pp. 3-11.

15. VanWick, A., Larralde, J., Lovell, CW and Chen, WF, “Development of a Pumping Prediction Model”, ASCE, *Journal of Transportation Engineering*, Vol. 115, No. 2, March, 1989, pp. 161–175.

16. Larralde, J. and Chen, WF, “Estimation of Mechanical Deterioration of Highway Rigid Pavements”, ASCE, *Journal of Transportation Engineering*, Vol. 113, No. 2, 1987, pp. 193–207

17. Bhatti, M.A., Barlow, J.A., and Stoner, J.W. “Modeling Damage to Rigid Pavements Caused by Subgrade Pumping,” ASCE, *Journal of Transportation Engineering*, Vol. 122, No. 1, Jan-Feb 1996, pp. 12-21.

18. Ashtiani, R., Little, D.N., Masad, E., “Material Factors That Influence Anisotropic Behavior of Aggregate Bases”, *Transportation Research Record No. 2059*, Transportation Research Board, Washington, D.C., 2008, pp. 20-30.

Appendix A: Parameters of the Deflection Basin

LIST OF APPENDIX A TABLES

Table A-1. Parameters of the Deflection Basin for Slab #1, East Joint, and Direction of Travel East to West

PASS No.	D_1	D_2	D_3	D_4	D_5	D_6	D_7	*AREA*
0	16.56	15.57	13.77	11.93	10.11	8.39	6.91	90.77
112	21.25	17.16	14.33	11.98	9.64	7.50	6.00	76.23
256	19.61	17.02	14.45	12.38	10.33	8.56	6.78	85.07
512	21.15	17.16	14.54	12.27	10.12	8.27	6.56	80.74
752	22.67	17.51	14.60	12.13	9.74	7.66	6.23	76.01
1008	22.72	16.95	14.29	11.92	9.47	7.39	6.15	74.60
1248	21.49	16.48	13.91	11.78	9.69	7.83	6.17	76.35
1504	20.83	16.99	14.41	12.20	10.01	8.28	6.41	80.11

Table A-2. Parameters of the Deflection Basin for Slab #1, West Joint, and Direction of Travel East to West

PASS No.	D_1	D_2	D_3	D_4	D_5	D_6	D_7	*AREA*
0	18.13	15.58	13.17	11.17	9.44	7.83	6.56	83.21
112	34.43	20.10	16.60	13.73	11.13	8.92	7.23	73.94
256	29.27	14.97	12.55	10.57	8.77	7.22	5.97	63.99
512	28.76	15.54	13.04	10.90	9.02	7.44	6.12	66.06
752	39.83	27.08	22.50	18.58	15.00	11.93	9.54	91.89
1008	37.89	19.72	16.36	13.60	10.95	8.77	7.18	71.06
1248	31.65	16.29	13.66	11.43	9.44	7.72	6.37	66.42
1504	24.89	15.84	13.37	11.26	9.36	7.76	6.41	72.23

Table A-3. Parameters of the Deflection Basin for Slab #2, East Joint, and Direction of Travel East to West

PASS No.	D_1	D_2	D_3	D_4	D_5	D_6	D_7	*AREA*
0	17.83	16.22	13.72	11.63	9.64	7.89	6.35	83.88
112	22.80	17.59	14.60	12.18	9.90	7.86	6.20	75.90
256	20.99	16.21	13.72	11.47	9.37	7.53	5.95	75.03
512	21.15	16.37	13.76	11.48	9.34	7.50	5.87	74.38
752	29.44	21.03	17.30	14.11	11.33	8.77	6.72	75.89
1008	25.97	17.36	14.39	11.96	9.65	7.66	5.95	69.90
1248	21.60	16.43	13.81	11.54	9.41	7.53	5.98	74.50
1504	20.39	17.12	14.39	12.03	9.78	7.85	6.24	79.44

Table A-4. Parameters of the Deflection Basin for Slab #2, West Joint, and Direction of Travel East to West

PASS No.	D_1	D_2	D_3	D_4	D_5	D_6	D_7	*AREA*
0	17.36	15.74	13.35	11.40	9.61	8.02	6.74	86.62
112	22.44	18.80	15.40	12.67	10.27	8.19	6.65	80.84
256	19.70	16.80	13.98	11.80	9.80	8.04	6.54	82.04
512	19.63	17.34	14.36	12.07	9.99	8.20	6.66	83.84
752	26.55	23.18	18.91	15.42	12.37	9.76	7.59	87.54
1008	22.99	19.57	16.03	13.25	10.72	8.62	6.86	82.75
1248	20.50	17.85	14.80	12.37	10.19	8.31	6.69	83.32
1504	20.11	17.32	14.41	12.11	10.05	8.28	6.72	83.42

Table A-5. Parameters of the Deflection Basin for Slab #3, East Joint, and Direction of Travel West to East

PASS No.	D_1	D_2	D_3	D_4	D_5	D_6	D_7	*AREA*
0	33.31	20.06	16.67	13.71	11.10	8.99	7.07	73.83
112	34.76	18.13	15.06	12.31	10.16	8.14	6.47	66.85
256	38.35	20.43	16.81	13.57	10.93	8.73	6.64	67.89
512	36.55	19.70	16.43	13.45	10.94	8.88	6.96	70.55
752	35.35	18.04	15.05	12.66	10.34	8.42	6.75	68.40
1008	35.94	20.98	17.45	14.15	11.46	9.20	6.98	72.33
1248	35.38	18.50	15.70	12.81	10.35	8.46	6.74	68.76
1504	33.91	20.17	16.80	13.43	10.93	8.85	7.06	73.20

Table A-6. Parameters of the Deflection Basin for Slab #3, West Joint, and Direction of Travel West to East

PASS No.	D_1	D_2	D_3	D_4	D_5	D_6	D_7	*AREA*
0	32.26	20.91	16.92	13.37	10.45	8.01	5.83	66.89
112	30.96	16.16	13.54	11.12	8.84	6.48	4.46	54.52
256	35.21	17.72	14.65	11.87	9.14	6.64	4.62	54.18
512	35.75	16.94	14.31	11.54	9.08	6.47	4.12	50.30
752	29.84	13.82	11.73	9.81	7.93	6.45	5.28	57.68
1008	37.52	17.21	14.45	11.74	9.18	6.85	4.75	53.51
1248	30.88	13.78	11.63	9.72	7.98	6.48	5.37	57.49
1504	30.04	14.07	12.07	10.13	8.40	6.99	5.65	60.54

Table A-7. Parameters of the Deflection Basin for Slab #3, East Joint, and Direction of Travel East to West

PASS No.	D_1	D_2	D_3	D_4	D_5	D_6	D_7	*AREA*
0	36.01	20.40	16.89	13.72	10.85	8.19	5.93	64.92
112	28.97	16.02	13.48	11.22	9.16	7.42	5.71	63.99
256	38.31	17.65	14.90	12.24	9.70	7.41	5.30	57.19
512	39.07	17.13	14.59	12.11	9.68	7.39	5.23	56.08
752	32.68	14.20	12.19	10.15	8.20	6.42	5.09	55.33
1008	41.47	18.59	15.65	12.87	10.25	7.75	5.31	56.70
1248	32.93	14.32	12.21	10.17	8.26	6.47	5.20	55.94
1504	29.15	17.43	14.58	12.17	9.69	7.71	5.80	66.15

Table A-8. Parameters of the Deflection Basin for Slab #3, West Joint, and Direction of Travel East to West

PASS No.	D_1	D_2	D_3	D_4	D_5	D_6	D_7	*AREA*
0	36.64	24.39	19.85	15.76	12.44	9.71	7.33	76.89
112	30.29	16.19	13.43	10.97	8.99	7.26	5.89	63.86
256	37.06	22.71	18.45	14.57	11.45	9.20	7.04	72.97
512	37.35	21.98	17.93	14.24	11.17	9.04	6.85	70.99
752	31.69	15.67	13.06	10.50	8.84	7.09	5.50	59.89
1008	37.61	24.47	19.99	15.81	12.43	9.65	7.45	76.97
1248	31.06	16.41	13.49	11.15	8.98	7.38	5.89	63.52
1504	30.11	16.38	13.69	11.20	9.07	7.48	5.98	64.92

Appendix B: Load Transfer Efficiency

LIST OF APPENDIX B TABLES

Table B-1. Load Transfer Efficiency for Slab #1, East Joint, Direction of Travel East to West

PASS No.	D_1	D_2	LTE_δ	*LTE**	LTE_σ	*LT*
0	16.56	15.57	0.94	0.97	0.50	0.33
112	21.25	17.16	0.81	0.89	0.35	0.26
256	19.61	17.02	0.87	0.93	0.41	0.29
512	21.15	17.16	0.81	0.90	0.35	0.26
752	22.67	17.51	0.77	0.87	0.31	0.24
1008	22.72	16.95	0.75	0.85	0.30	0.23
1248	21.49	16.48	0.77	0.87	0.35	0.26
1504	20.83	16.99	0.82	0.90	0.36	0.26

Table B-2. Load Transfer Efficiency for Slab #1, West Joint, Direction of Travel East to West

PASS No.	D_1	D_2	LTE_δ	*LTE**	LTE_σ	*LT*
0	18.13	15.58	0.86	0.92	0.40	0.28
112	34.43	20.10	0.58	0.74	0.19	0.16
256	29.27	14.97	0.51	0.68	0.16	0.14
512	28.76	15.54	0.54	0.70	0.17	0.15
752	39.83	27.08	0.68	0.81	0.25	0.20
1008	37.89	19.72	0.52	0.68	0.16	0.14
1248	31.65	16.29	0.51	0.68	0.16	0.14
1504	24.89	15.84	0.64	0.78	0.22	0.18

Table B-3. Load Transfer Efficiency for Slab #2, East Joint, Direction of Travel East to West

PASS No.	D_1	D_2	LTE_δ	*LTE**	LTE_σ	*LT*
0	17.83	16.22	0.91	0.95	0.45	0.31
112	22.80	17.59	0.77	0.87	0.31	0.24
256	20.99	16.21	0.77	0.87	0.31	0.24
512	21.15	16.37	0.77	0.87	0.31	0.24
752	29.44	21.03	0.71	0.83	0.27	0.21
1008	25.97	17.36	0.67	0.80	0.24	0.19
1248	21.60	16.43	0.76	0.86	0.30	0.23
1504	20.39	17.12	0.84	0.91	0.38	0.27

Table B-4. Load Transfer Efficiency for Slab #2, West Joint, Direction of Travel East to West

PASS No.	D_1	D_2	LTE_δ	*LTE**	LTE_σ	*LT*
0	17.36	15.74	0.91	0.95	0.45	0.31
112	22.44	18.80	0.84	0.91	0.38	0.27
256	19.70	16.80	0.85	0.92	0.39	0.28
512	19.63	17.34	0.88	0.94	0.42	0.29
752	26.55	23.18	0.87	0.93	0.41	0.29
1008	22.99	19.57	0.85	0.92	0.39	0.28
1248	20.50	17.85	0.87	0.93	0.41	0.29
1504	20.11	17.32	0.86	0.93	0.40	0.28

Table B-5. Load Transfer Efficiency for Slab #3, East Joint, Direction of Travel West to East

PASS No.	D_1	D_2	LTE_δ	*LTE**	LTE_σ	*LT*
0	33.31	20.06	0.60	0.75	0.20	0.17
112	34.76	18.13	0.52	0.69	0.16	0.14
256	38.35	20.43	0.53	0.70	0.17	0.14
512	36.55	19.70	0.54	0.70	0.17	0.15
752	35.35	18.04	0.51	0.68	0.16	0.14
1008	35.94	20.98	0.58	0.74	0.19	0.16
1248	35.38	18.50	0.52	0.69	0.16	0.14
1504	33.91	20.17	0.59	0.75	0.20	0.16

Table B-6. Load Transfer Efficiency for Slab #3, West Joint, Direction of Travel West to East

PASS No.	D_1	D_2	LTE_δ	*LTE**	LTE_σ	*LT*
0	32.26	20.91	0.65	0.79	0.23	0.19
112	30.96	16.16	0.52	0.69	0.16	0.14
256	35.21	17.72	0.50	0.67	0.15	0.13
512	35.75	16.94	0.47	0.64	0.14	0.12
752	29.84	13.82	0.46	0.63	0.14	0.12
1008	37.52	17.21	0.46	0.63	0.14	0.12
1248	30.88	13.78	0.45	0.62	0.13	0.12
1504	30.04	14.07	0.47	0.64	0.14	0.12

Table B-7. Load Transfer Efficiency for Slab #3, East Joint, Direction of Travel East to West

PASS No.	D_1	D_2	LTE_δ	*LTE**	LTE_σ	*LT*
0	36.01	20.40	0.57	0.72	0.19	0.16
112	28.97	16.02	0.55	0.71	0.18	0.15
256	38.31	17.65	0.46	0.63	0.14	0.12
512	39.07	17.13	0.44	0.61	0.13	0.12
752	32.68	14.20	0.43	0.61	0.13	0.11
1008	41.47	18.59	0.45	0.62	0.13	0.12
1248	32.93	14.32	0.43	0.61	0.13	0.11
1504	29.15	17.43	0.60	0.75	0.20	0.17

Table B-8. Load Transfer Efficiency for Slab #3, West Joint, Direction of Travel East to West

PASS No.	D_1	D_2	LTE_δ	*LTE**	LTE_σ	*LT*
0	36.64	24.39	0.67	0.80	0.24	0.19
112	30.29	16.19	0.53	0.70	0.17	0.14
256	37.06	22.71	0.61	0.76	0.21	0.17
512	37.35	21.98	0.59	0.74	0.20	0.16
752	31.69	15.67	0.49	0.66	0.15	0.13
1008	37.61	24.47	0.65	0.79	0.23	0.19
1248	31.06	16.41	0.53	0.69	0.17	0.14
1504	30.11	16.38	0.54	0.70	0.17	0.15

Appendix C: Joint Load Transfer

LIST OF APPENDIX C FIGURES

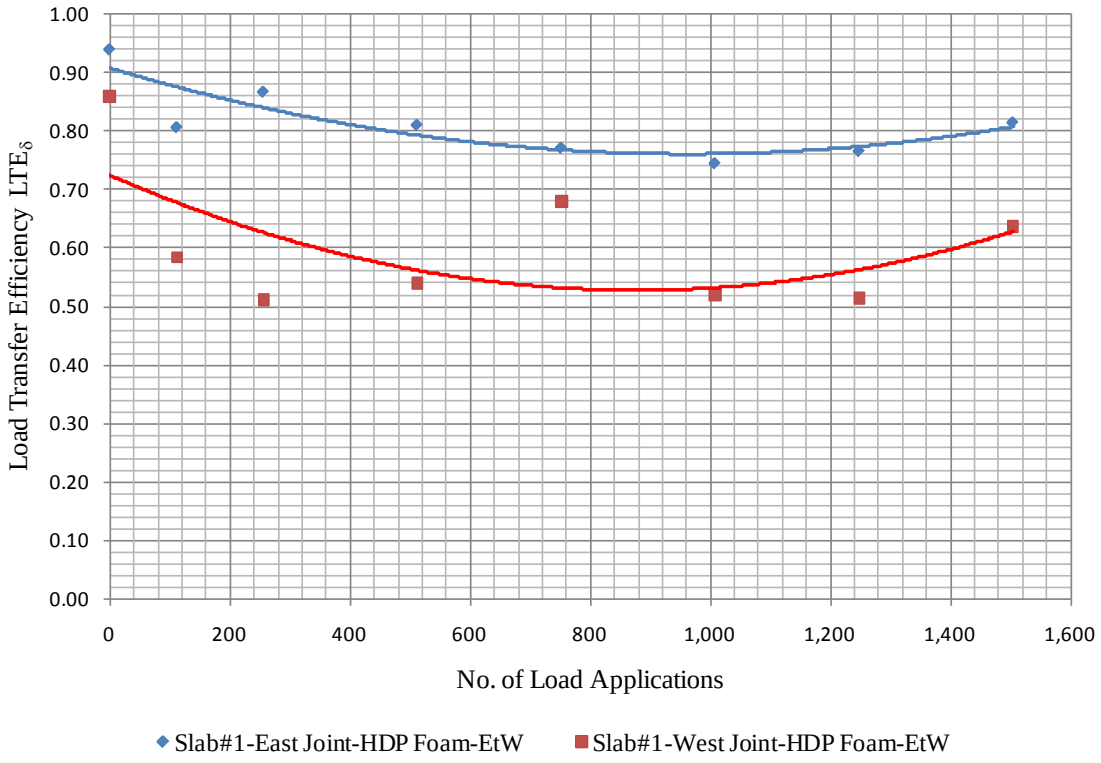

Figure C-1. Load Transfer Efficiency (LTE_{δ}) for Slab #1

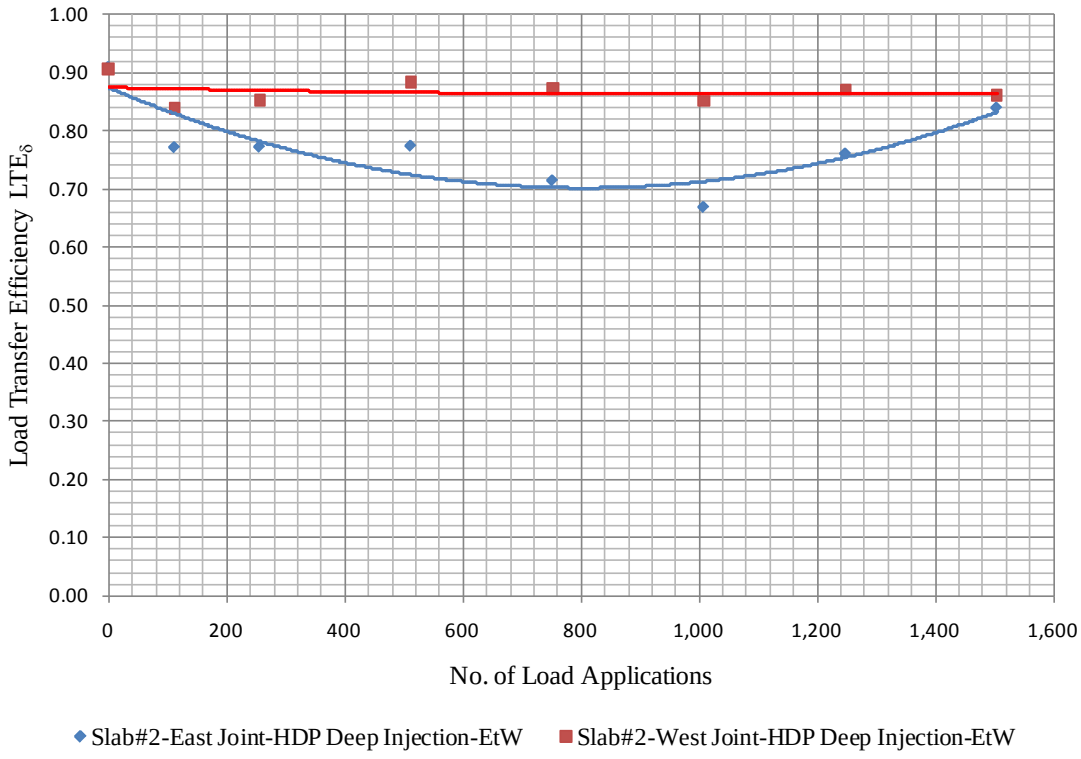

Figure C-2. Load Transfer Efficiency (LTE_{δ}) for Slab #2

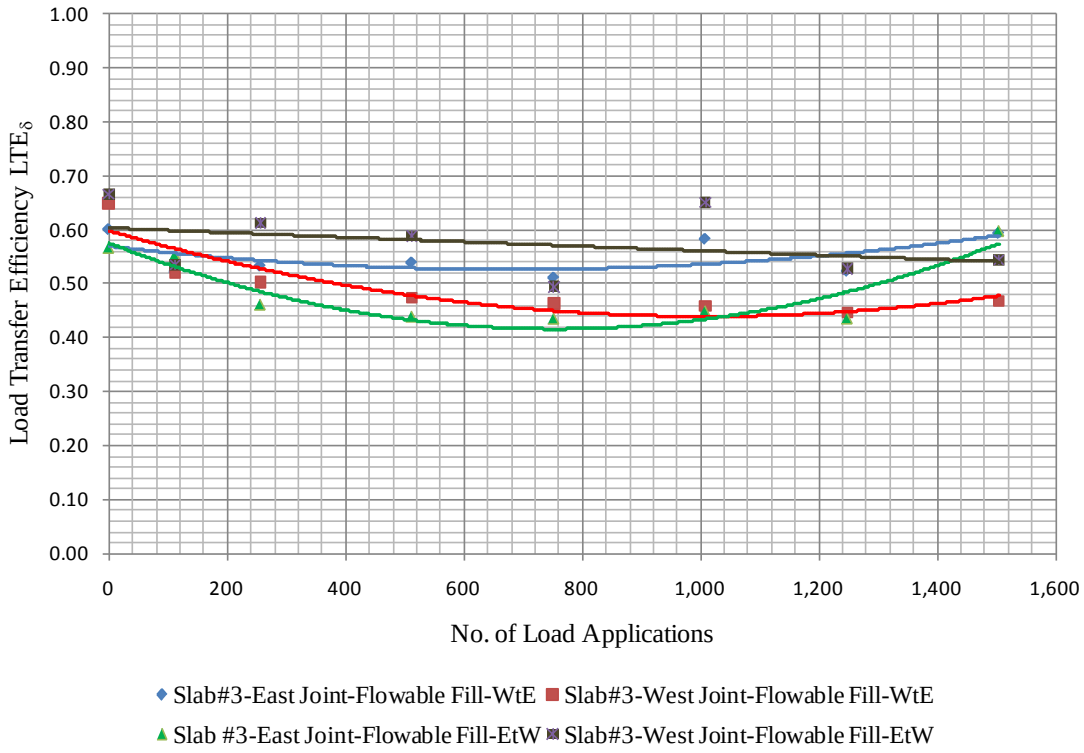

Figure C-3. Load Transfer Efficiency (LTE$_\delta$) for Slab #3

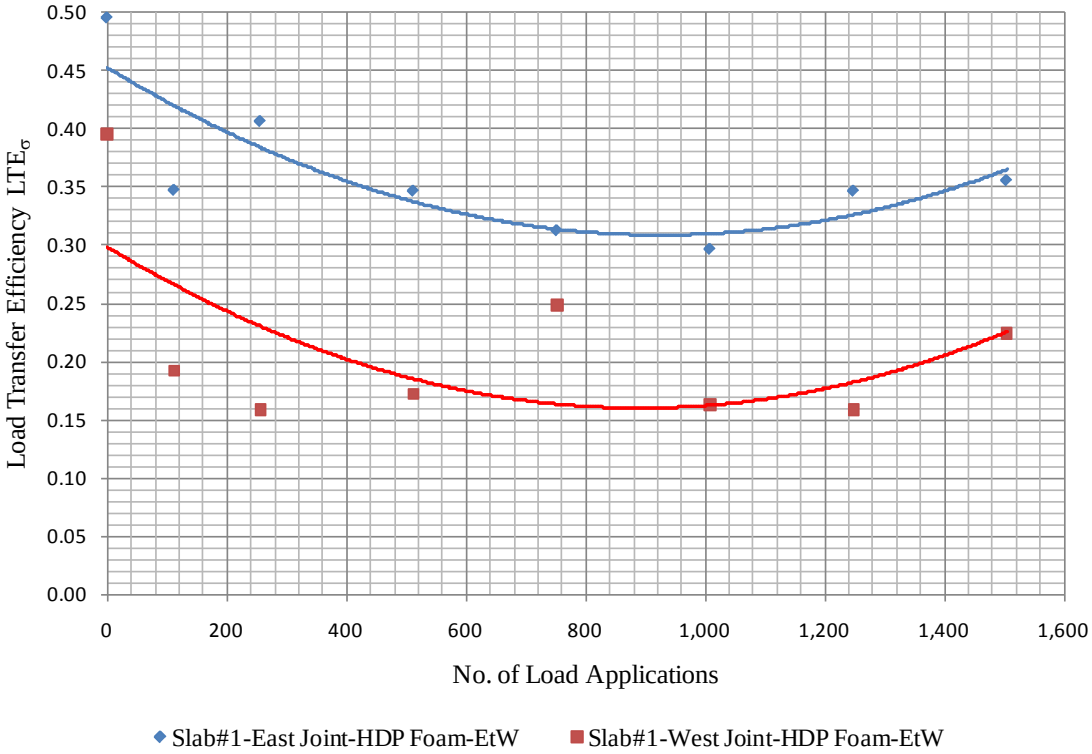

Figure C-4. Load Transfer Efficiency (LTE$_\sigma$) for Slab #1

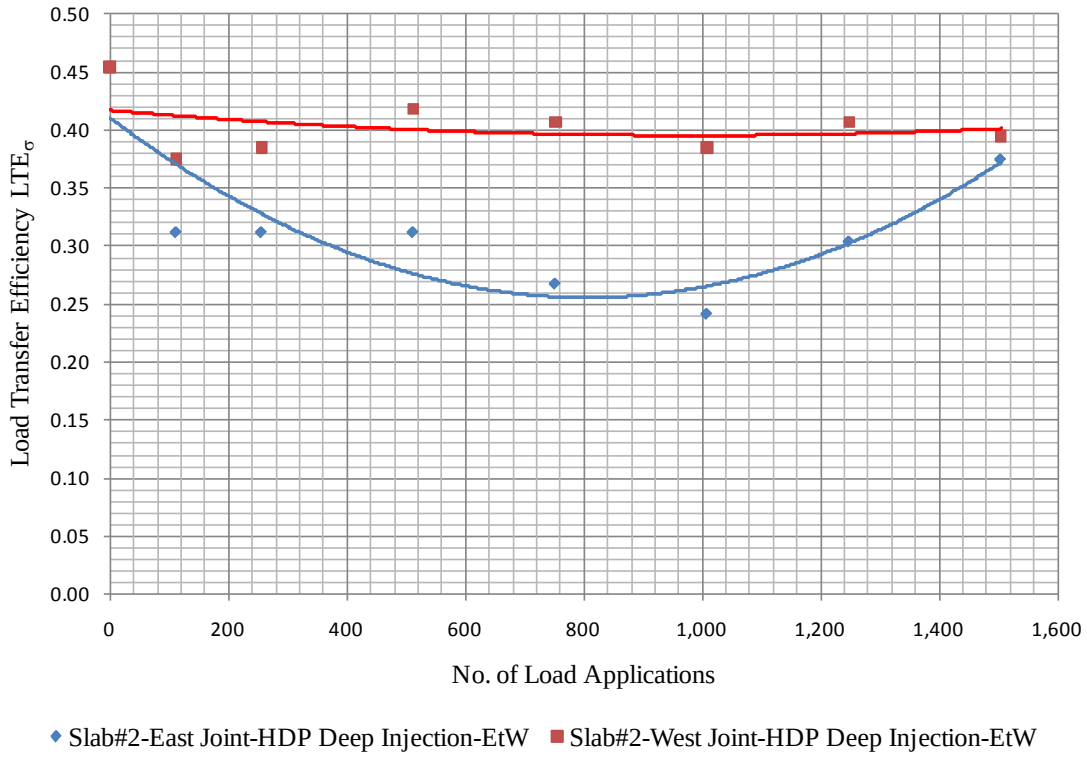

Figure C-5. Load Transfer Efficiency (LTE_σ) for Slab #2

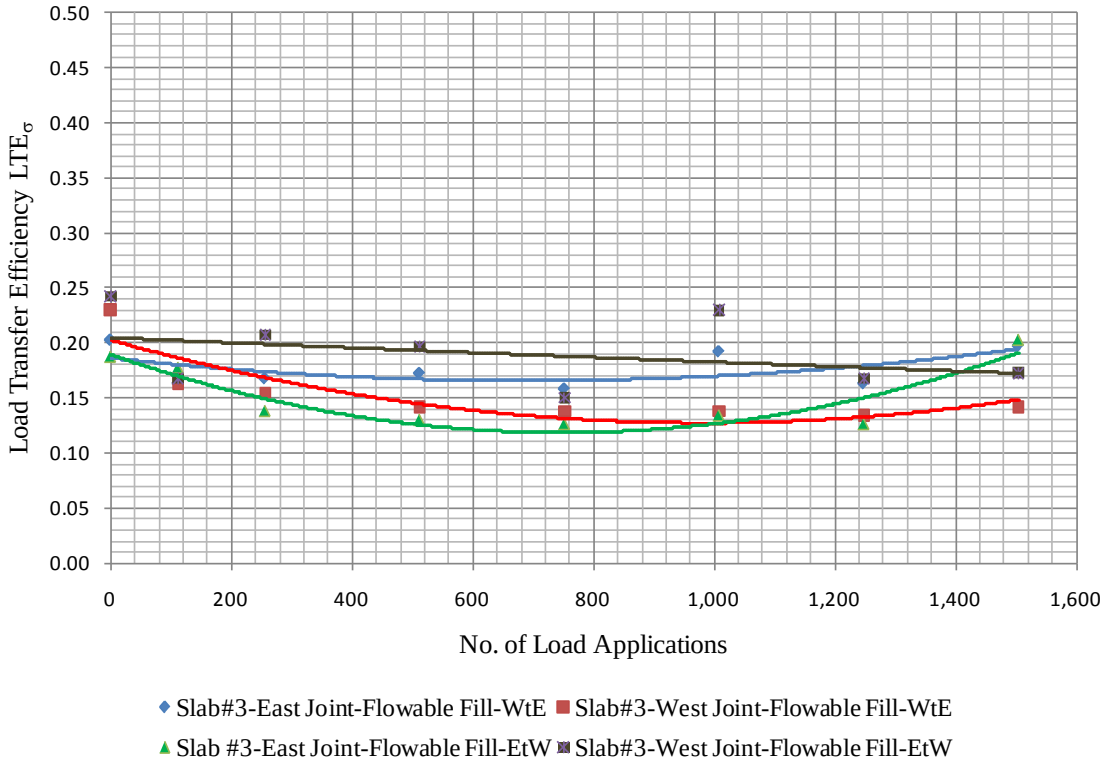

Figure C-6. Load Transfer Efficiency (LTE_σ) for Slab #3

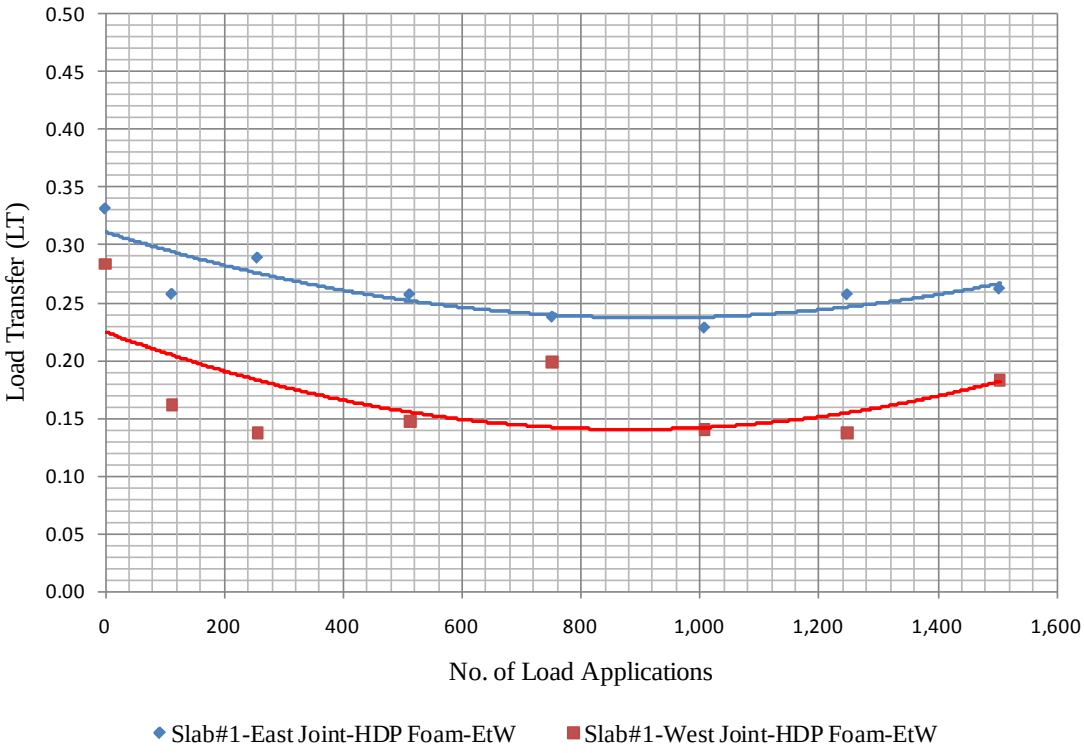

Figure C-7. FAA Criteria for Load Transfer Efficiency (LT) for Slab #1

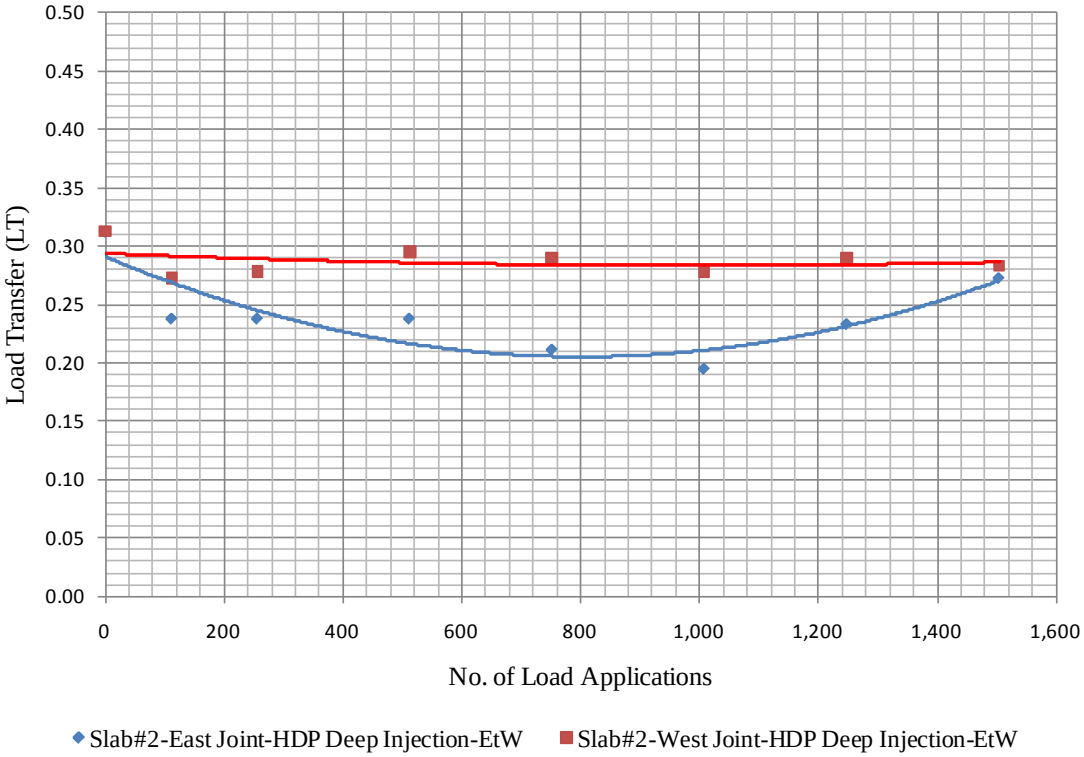

Figure C-8. FAA Criteria for Load Transfer Efficiency (LT) for Slab #2

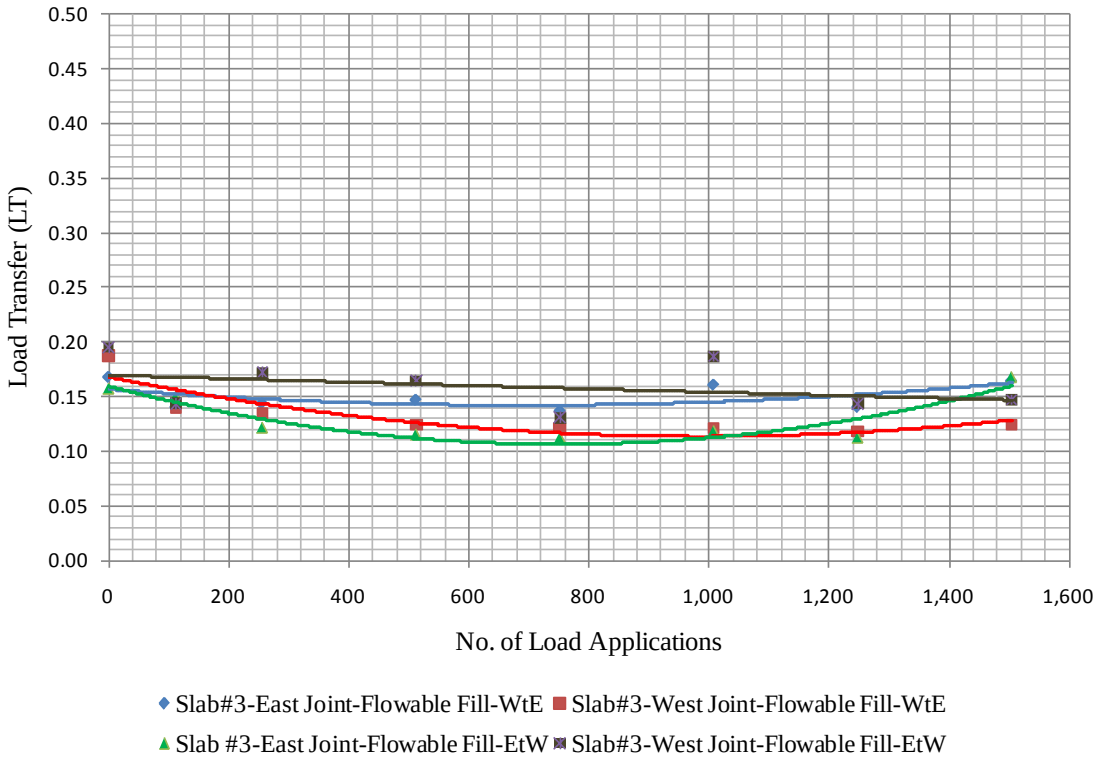

Figure C-9. FAA Criteria for Load Transfer Efficiency (LT) for Slab #3

LIST OF SYMBOLS, ABBREVIATIONS, AND ACRONYMS

ADR	airfield damage repair
AFRL	Air Force Research Laboratory
AOS	Aircraft Operating Surfaces
ASTM	American Society of Testing and Materials
DE	differential energy
FAA	Federal Aviation Administration
FE	finite element
FWD	falling weight deflectometer
HDP	high-density polyurethane
HWD	heavy-weight deflectometer
kN	kilonewtons
ksi	kips per square inch
lbf	pounds force
LT	FAA Criteria for load transfer efficiency
LTE	load transfer efficiency
LTE_{AGG}	load transfer through aggregate interlock
LTE_{Dowel}	load transfer through reinforcement
$LTE_{Foundation}$	load transfer through foundation support
LTE_{Total}	total load transfer efficiency provided by aggregate interlock, steel reinforcement and foundation support
LTE_{δ}	deflection based load transfer efficiency
LTE_{σ}	stress based load transfer efficiency
MEPDG	Mechanistic Empirical Pavement Design Guide
PCC	Portland cement concrete
pci	pounds per cubic inch
psi	pounds per square inch